01 Apr 2010

CH_3CH_2OD/D_2O Binary Condensation in a Supersonic Laval Nozzle: Presence of Small Clusters Inferred from a Macroscopic Energy Balance

Shinobu Tanimura

Barbara E. Wyslouzil

Gerald Wilemski
Missouri University of Science and Technology, wilemski@mst.edu

CH_3CH_2OD/D_2O binary condensation in a supersonic Laval nozzle: Presence of small clusters inferred from a macroscopic energy balance

Shinobu Tanimura,[1,a)] Barbara E. Wyslouzil,[1] and Gerald Wilemski[2]
[1]*Department of Chemical and Biomolecular engineering, The Ohio State University, 140 West 19th Av., Columbus, Ohio 43210, USA*
[2]*Department of Physics, Missouri University of Science and Technology, Rolla, Missouri 65409-0640, USA*

(Received 15 September 2009; accepted 22 February 2010; published online 8 April 2010)

We determined the heat released in the condensing flow of a CH_3CH_2OD/D_2O/carrier gas mixture ($EtOD/D_2O$ for brevity) through a supersonic Laval nozzle by integrating the equations for supersonic flow with condensation, using the static pressure, temperature, and mole fractions of EtOD and D_2O monomers [S. Tanimura, B. E. Wyslouzil, M. S. Zahniser, *et al.*, J. Chem. Phys. **127**, 034305 (2007)] as inputs. By considering the depletion of the monomer species, the deviation of the pressure from the isentropic value, and the heat released, we estimated that ~10% of the EtOD molecules are present as pure clusters (dimer to tetramer) upstream of the onset point of condensation. In contrast, clustering was not detected when only pure EtOD was present under the same conditions (temperature and the partial pressure of EtOD) for which clustering was observed in the $EtOD/D_2O$ flow. This suggests that the formation of EtOD clusters is facilitated by D_2O in the $EtOD/D_2O$ flow. A comparison of the heat released to the flow and the expected heat of dissociation of the $EtOD/D_2O$ droplets suggests that small EtOD clusters persist downstream of the onset point. Both upstream and downstream of the onset point of condensation, the concentration of these clusters in the nozzle is higher than that expected at equilibrium. A possible mechanism for the overabundance of pure EtOD clusters is that they form in the mixed $EtOD/D_2O$ particles (droplets or clusters) and evaporate from them. © *2010 American Institute of Physics*.
[doi:10.1063/1.3360304]

I. INTRODUCTION

When water and alcohol cocondense, particle formation and growth are complicated by several effects. These include the nonideality of the liquid mixtures, enrichment of the surface by the alcohol, and, in the case of ethanol and methanol, the potential for significant association (clustering) of the alcohol in the gas phase. To study this problem in detail we developed a supersonic nozzle apparatus that reliably produces a high number density aerosol comprised of droplets with radii generally less than 10 nm under steady flow conditions. Condensation in the nozzle is characterized as a function of axial position by measuring the static pressure using a static pressure probe,[1] and the mole fraction(s) of the condensable vapor(s) and the average temperature of the carrier gas using tunable diode laser absorption spectroscopy (TDLAS).[2–4] The aerosol is characterized by small angle x-ray[5] (or neutron)[6,7] scattering (SAXS or SANS) experiments to determine the average size, distribution width, and number density. Because the gas velocity is 300–500 m/s under typical operating conditions we can observe the progress of the condensation process with a time resolution of about 0.5 μs by changing the measurement position. Furthermore, we can obtain high signal-to-noise ratios by accumulating measurements under the steady flow conditions.

In our earlier work on the condensation of D_2O we showed that, on average, the energy released to the flow downstream of the onset of condensation was in good agreement with the bulk heat of vaporization for subcooled D_2O.[3] In this paper we extend the energy balance approach to our binary condensation results for $EtOD/D_2O$.[4] When we compare the values of the expected and observed heat release downstream of onset, we find that the latter is about 3 kJ/(mol condensate) lower than the expected value of about 50 kJ/(mol condensate). This difference is consistent with ~10% of the total EtOD persisting as small gas phase clusters rather than as droplets. Mass spectroscopic measurements of evaporating ethanol/water droplets[8,9] suggest that evaporation of small ethanol-dominant clusters from ethanol/water droplets is a possible route for producing clusters when they should not exist under the equilibrium assumption. Our own preliminary Fourier transform infrared spectroscopy (FTIR) experiments provide additional evidence for the presence of ethanol dimer at levels higher than predicted by equilibrium calculations.

The organization of this paper is as follows. In Sec. II we briefly review the relevant experimental techniques used to derive the measured quantities including the static pressure p, the average temperature $\langle T \rangle$ and the composition of the flowing gas, and the size distribution parameters of the aerosol. We summarize the analysis methods in Sec. III with more detailed derivations presented in the Appendices. The results of the analysis are presented in Sec. IV and, finally, in Sec. V, we summarize our work.

[a)]Electronic mail: tanimura5@yahoo.co.jp.

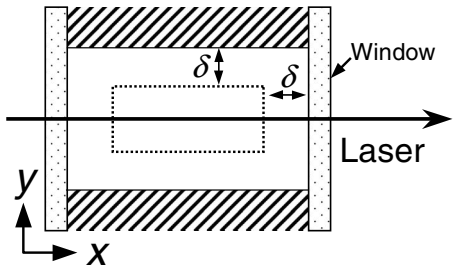

FIG. 1. A cross section of the supersonic nozzle. δ denotes the disturbance thickness of boundary layer.

II. EXPERIMENTAL

The analysis presented here is based on (1) our axially resolved static pressure and TDLAS measurements published earlier,[4] and (2) our SAXS experiments that are described in detail in Ref. 5. Thus, here we only summarize the experimental methods very briefly.

A. Pressure trace measurements and TDLAS measurements

In the current experiments, a gas mixture (N_2+CH_4 +EtOD+D_2O) expands in a supersonic Laval nozzle from a stagnation temperature T_0=303.7 K and stagnation pressure p_0=30.2 kPa. The initial composition of the mixture is $(y_{CH_4})_0$=0.0406, $(y_{EtOD})_0$=0.0097, and $(y_{D_2O})_0$=0.0146, where y_i is the mole fraction of component i, and N_2 comprises the balance of the flow. As the temperature and pressure decrease in the nozzle, the vapor phase becomes highly supersaturated, and, at some point, particle formation and growth rapidly deplete the condensable material (EtOD +D_2O) from the vapor phase. Methane does not condense under our operating conditions. Rather, we use it to determine the temperature of the gas mixture in the TDLAS measurements, or LAM, for short.

In a pressure trace measurement (PTM), we measure the static pressure p along the centerline of the nozzle using a movable static pressure probe. In the LAM, an infrared beam crosses the nozzle perpendicular to the gas flow through CaF_2 windows in the flat sidewalls and is detected using a liquid N_2 cooled $Hg_{1-x}Cd_xTe$ (MCT) detector. The Voigt line profiles are fitted to the CH_4 and D_2O absorption lines to determine the absorbance area. The concentration of EtOD monomer in the condensing flow is determined by comparing the spectrum measured in the condensing flow with that measured in a noncondensing flow of pure EtOD at the same temperature and pressure as in the condensing flow and at a known concentration. The average temperature $T_{LAM}=\langle T\rangle$ is determined from the area ratio of two CH_4 peaks with different ground state energies, where $\langle T\rangle$ denotes the averaged temperature along the IR laser light path. This temperature is higher than the centerline temperature T because of the presence of boundary layers along the nozzle walls (see Fig. 1).

B. Small angle x-ray scattering measurements

The x-ray scattering measurements (XSM) were performed using the SAXS facility on the Besserc 12-ID beamline at the Advanced Photon Source (APS) at Argonne National Laboratory. We used a 0.2×0.2 mm^2 beam of 12 keV x rays with a wavelength spread of $\Delta\lambda/\lambda=10^{-4}$. The experimental setup is similar to that used in the LAM, but the windows are 25 μm thick mica. The two-dimensional scattering pattern was recorded using a charge coupled device (CCD) array and the data were reduced to determine the one-dimensional scattering spectrum using the APS data inversion program. The spectra were fit using a normalized Schultz distribution of well mixed spheres,[10]

$$\tilde{n}(r)=\left(\frac{Z+1}{\langle r\rangle}\right)^{Z+1}r^Z\exp\left[-\left(\frac{Z+1}{\langle r\rangle}\right)r\right]\frac{1}{\Gamma(Z+1)},\quad Z>-1, \tag{1}$$

to determine the average particle size $\langle r\rangle$, and polydispersity, $\xi=s/\langle r\rangle=(Z+1)^{-1/2}$, of the aerosol, where Γ is the gamma function, and s is the standard deviation of r.

III. THERMODYNAMIC ANALYSIS OF NOZZLE FLOW WITH CONDENSATION

A. The supersonic flow equations with condensation/clustering

The equations that describe adiabatic supersonic flow with condensation or clustering are based on the conservation equations[11(a)] for mass,

$$\rho uA=\text{const}, \tag{2}$$

momentum,

$$\rho u du=-dp, \tag{3}$$

and energy,

$$h+u^2/2=h_0, \tag{4}$$

together with an equation of state for the fluid,

$$p=\rho\left\{\frac{\omega_{\text{inert}}}{\mu_{\text{inert}}}+\sum_i\left(\frac{\omega_{vi}}{\mu_{vi}}\right)+\frac{\omega_{cls}}{\langle\mu_{cls}\rangle}+\frac{\omega_c}{\langle\mu_c\rangle}\right\}RT. \tag{5}$$

In Eqs. (2)–(5), ρ is the mass density, u is the velocity, A is the effective flow area, p is the static pressure, h is the enthalpy per unit mass of the gas mixture, including the condensate, and h_0 is the value of h at the stagnation condition. The molecular weight and mass fraction are μ and ω, respectively. The subscripts, inert, vi, cls, and c denote the inert carrier gas, the condensable vapor of species i, the small clusters, and the condensate (droplets), respectively. The angle brackets $\langle\cdots\rangle$ indicate the number-averaged value. In this study, we make the standard assumption that the term $\omega_c/\langle\mu_c\rangle$ can be neglected because the average molecular weight of the droplets $\langle\mu_c\rangle$ is large. For systems like ethanol and methanol, where clustering in the gas phase can be significant, the contribution of $\omega_{cls}/\langle\mu_{cls}\rangle$ may be important, and the effect of this term is considered in Sec. IV C.

When condensation and/or clustering occur in the nozzle h can be expressed as

$$h = h_0 + \int_{T_0}^{T} c^0_{p\text{-gas}} dT - q, \tag{6}$$

where q is the heat released to the gas mixture by the phase change and/or cluster formation, per unit mass of the system, that is, q is the heat of dissociation of the droplets or the heat of dissociation of the clusters. $c^0_{p\text{-gas}}$ is the isobaric heat capacity per unit mass of the gas mixture in the fictitious state where neither condensation nor clustering occurs, and expressed by

$$c^0_{p\text{-gas}} = \omega_{\text{inert}} c_{p\text{-inert}} + \sum_i \omega_i c^0_{p-i(v)}. \tag{7}$$

Here $c_{p\text{-inert}}$ is the isobaric heat capacity per unit mass of carrier gas, and $c^0_{p-i(v)}$ is that of condensable species i in the ideal gas state (i.e., at infinitely low density). The mass fractions of the condensable species i, ω_i, and the inert gas ω_{inert} are constant. We assume $c_{p\text{-inert}}$ is constant and $c^0_{p-i(v)}$ depends solely on the temperature, and, thus, $c^0_{p\text{-gas}}$ is a function of only the temperature. Differentiating Eqs. (4) and (6) gives

$$c^0_{p\text{-gas}} dT - d(q) + u du = 0. \tag{8}$$

We note that for binary condensation q reflects the contributions due to the heat of vaporization of the pure components, the heat of mixing, the surface energy, as well as any change in enthalpy due to the difference in temperature between the droplets and the gas, and the heat of dissociation of small gas-phase clusters.

Equations (2), (3), (5), and (8) may be combined to yield the supersonic flow equations, Eqs. (9)–(12), given below.

$$d\left(\frac{\rho}{\rho_0}\right) = \left[\frac{1}{\gamma_m}\left(\frac{u^*}{u}\right)^2 \frac{T_0}{T^*}\right] d\left(\frac{p}{p_0}\right) - \left(\frac{\rho}{\rho_0}\right) d \ln\left(\frac{A}{A^*}\right), \tag{9}$$

$$d\left(\frac{T}{T_0}\right) = \frac{\rho_0}{\rho}\left[w_0(g) - \frac{1}{\gamma_m}\left(\frac{u^*}{u}\right)^2 \frac{T}{T^*}\right] d\left(\frac{p}{p_0}\right) + \left(\frac{T}{T_0}\right) \times \left[d \ln\left(\frac{A}{A^*}\right) + \sum_i w_i(g) dg_i\right], \tag{10}$$

$$\frac{d(q)}{c^0_{p\text{-gas}} T_0} - \frac{T}{T_0} \sum_i w_i(g) dg_i = \frac{\rho_0}{\rho}\left[\eta_{\text{gas}}(g) - \frac{1}{\gamma_m}\left(\frac{u^*}{u}\right)^2 \frac{T}{T^*}\right] d\left(\frac{p}{p_0}\right) + \left(\frac{T}{T_0}\right) d \ln\left(\frac{A}{A^*}\right), \tag{11}$$

$$u = \frac{u^* \rho^* A^*}{\rho A}. \tag{12}$$

In Eqs. (9)–(12) the subscript zero indicates the value at the nozzle inlet (stagnation conditions), the asterisk denotes the values of the variable at the nozzle throat, and γ_m is the specific heat ratio of the gas mixture at the throat. The quantities g, $w_0(g)$, $w_i(g)$, and $\eta_{\text{gas}}(g)$ are defined by

$$g \equiv \sum_i g_i, \tag{13}$$

$$w_0(g) \equiv \mu/[\mu_0(1-g)], \tag{14}$$

$$w_i(g) \equiv \mu/[\mu_{vi}(1-g)], \tag{15}$$

$$\eta_{\text{gas}}(g) \equiv w_0(g) - \frac{c^0_{p\text{-gas},0}}{c^0_{p\text{-gas}}}\left(\frac{\gamma_0 - 1}{\gamma_0}\right), \tag{16}$$

where g_i is the mass fraction of condensate of species i, μ is the mean molecular weight of the gas mixture, excluding the condensate or clusters, μ_0 is the value of μ at the stagnation conditions, and μ_{vi} is the molecular weight of condensable species i. Finally, $c^0_{p\text{-gas},0}$ in Eq. (16) is the value of $c^0_{p\text{-gas}}$ at the stagnation conditions, i.e., $c^0_{p\text{-gas},0} = c^0_{p\text{-gas}}(T_0)$, and γ_0 is the specific heat ratio of the gas mixture at those conditions. Equation (16) was derived assuming that there is no condensation or clustering under the stagnation conditions. When deriving Eqs. (9)–(16), the term $\omega_{cls}/\langle\mu_{cls}\rangle$ in Eq. (5) was neglected.

The difference between the flow equations presented here and those presented earlier[3] lies in Eq. (8). In our previous work, we restricted the application of the flow equations to the one-component condensation and assumed

$$q = gL, \tag{17}$$

where L is the heat of vaporization of the condensable species per unit mass. In this case Eq. (8) may be written as

$$c_p dT - L dg + u du = 0, \tag{18}$$

where c_p is the isobaric heat capacity of the gas mixture, including the condensate, per unit mass, given by

$$c_p = \omega_{\text{inert}} c_{p\text{-inert}} + (\omega - g) c^0_{p(v)} + g c_{p(l)}, \tag{19}$$

and the subscript l indicates the liquid. It is noted that, in the derivation of Eq. (18), $dL/dT = c^0_{p(v)} - c_{p(l)}$ (Kirchhoff's equation)[12] was used assuming $\partial L/\partial p = 0$. These simplifications yield Eqs. (20) and (21) instead of Eqs. (11) and (16).

$$\left[\frac{L}{c_p T_0} - \frac{T}{T_0} w(g)\right] dg = \frac{\rho_0}{\rho}\left[\eta(g) - \frac{1}{\gamma_m}\left(\frac{u^*}{u}\right)^2 \frac{T}{T^*}\right] d\left(\frac{p}{p_0}\right) + \left(\frac{T}{T_0}\right) d \ln\left(\frac{A}{A^*}\right), \tag{20}$$

$$\eta(g) \equiv w_0(g) - \frac{c^0_{p\text{-gas},0}}{c_p}\left(\frac{\gamma_0 - 1}{\gamma_0}\right). \tag{21}$$

When we solve Eqs. (9)–(12) in this study, the pressure p, temperature T, and the mass fraction of each condensing species g_i are the input variables while density ρ, effective area ratio A/A^*, velocity u, and the heat released by clustering or droplet formation, q, are the derived quantities.

B. Effect of the boundary layer on LAM

In the supersonic nozzle, momentum and thermal boundary layers develop along the surfaces, and, as illustrated in Fig. 1, the laser light crosses two boundary layers during each measurement. In the thermal boundary layer, the temperature of the gas is higher than the temperature at the center of the flow, T, i.e., the temperature that appears in the

supersonic flow equations.[3] The temperature determined by laser absorption measurements, T_{LAM}, is, therefore, higher than T and equals the average temperature of the gas along the laser light path, $\langle T\rangle$.

To determine q from the supersonic flow equations, we need a way to use the measured values T_{LAM} as input rather than the desired quantity T. We first set T equal to T_{LAM}, and determine A/A^* (and the other variables) by integrating Eqs. (9)–(12) using p and g_i as the other known variables. From the values of A/A^* and the physical dimensions of the nozzle, we determine the boundary layer thickness and find T so that $\langle T\rangle = T_{\mathrm{LAM}}$ at each point in the nozzle. We then use the new estimates of T as input to the flow equation and iterate until the absolute differences between the consecutive estimates of T at all points are less than 0.1 K. The solution usually converges within two or three iterations. To determine the $\langle T\rangle$, the temperature profile in the laminar (turbulent) boundary layer was used in the region of decreasing (increasing) pressure as detailed in Appendix A.

In the isentropic flow (carrier gas flow without condensable species), T and $\langle T\rangle$ can be determined only from the PTM, and the value of $\langle T\rangle$ agreed with T_{LAM} within an error of 1 K in our previous study.[4] Hence we estimated the uncertainty in the determination of T_{LAM} to be 1 K.

In contrast with the temperature measurements, the mole fractions of EtOD, D_2O, or CH_4, determined by LAM are not affected by temperature nonuniformity across the flow because the temperature dependencies of the total molar density and the molar density of each species are the same, and the thermal diffusion effects are negligible under the conditions of these experiments.

C. Estimating the heat of dissociation for binary droplets from the bulk thermodynamic properties of EtOD/D_2O mixtures

As the EtOD/D_2O droplets grow, they release heat to the flowing gas stream. The major contribution to the heat release is the heat of vaporization of the pure components. Other effects that modify the observed value of q include the heat of mixing between EtOD and D_2O, the surface energy of the droplets, and the difference in temperature between the droplets (T_{drop}) and the gas phase (T_{gas}) when the droplets are growing rapidly. One should also account for surface enrichment effects in these droplets by distinguishing between the average composition of the droplets x^{av} and their interior or bulk composition x^b. Finally, ethanol is known to form clusters, in particular, dimers and tetramers, in the gas phase[13] and this process also releases heat to the gas mixture.

As detailed in Appendix B, the molar heat of dissociation of the multicomponent droplets can be written as

$$\begin{aligned}\Delta h_{\mathrm{theor}} = {} & x^{\mathrm{av}}\Delta h^{\mathrm{bulk}}_{\mathrm{vap\text{-}EtOD}}(T_{\mathrm{drop}},x^b) \\ & + (1-x^{\mathrm{av}})\Delta h^{\mathrm{bulk}}_{\mathrm{vap\text{-}D2O}}(T_{\mathrm{drop}},x^b) \\ & - \{\sigma(T_{\mathrm{drop}},x^b) - T_{\mathrm{drop}}(\partial\sigma/\partial T)\}a \\ & - \int_{T_{\mathrm{gas}}}^{T_{\mathrm{drop}}} \{x^{\mathrm{av}}C^0_{p\text{-EtOD}(v)} + (1-x^{\mathrm{av}})C^0_{p-\mathrm{D_2O}(v)}\}dT, \quad (22)\end{aligned}$$

where $\Delta h^{\mathrm{bulk}}_{\mathrm{vap}\text{-}i}$ is the partial molar heat of vaporization of species i in the EtOD/D_2O bulk liquid, σ is the surface tension, a is the surface per mol of condensate, and $C^0_{p-i(v)}$ is the isobaric molar heat capacity of species i in the vapor phase. T_{drop} was estimated from an energy balance on the droplets as outlined in Appendix B. Correlations for the physical properties required to evaluate $\Delta h_{\mathrm{theor}}$ are summarized in Appendix C.

The average mole fraction of EtOD of the droplets is directly determined from the LAM as

$$x^{\mathrm{av}} = \frac{g_{\mathrm{EtOD}}/\mu_{\mathrm{EtOD}}}{g_{\mathrm{EtOD}}/\mu_{\mathrm{EtOD}} + g_{\mathrm{D_2O}}/\mu_{\mathrm{D_2O}}}, \quad (23)$$

where g_i and μ_i are the mass fraction of condensate and the molecular weight of species i. The bulk composition x^b and the surface mole fraction x^s of the droplets are derived from the x^{av} and the droplet radius r using the explicit cluster model by Laaksonen and Kulmala.[14] The droplet radius is determined from the XSM.

To account for the difference in temperature between the LAM and the XSM, the $\langle r(z)\rangle$ data were shifted upstream by 0.34 cm as described in Appendix D. Furthermore, when $z<1.83$ cm, the x-ray scattering intensity was too low to directly determine $\langle r(z)\rangle$ and, thus, in this region we extrapolated $\langle r(z)\rangle$ from the value measured at $z_{\mathrm{ref}}=1.83$ cm using

$$\begin{aligned}&\langle r(z)\rangle = \langle r(z_{\mathrm{ref}})\rangle\{V_c(z)/V_c(z_{\mathrm{ref}})\}^{1/3}, \\ &V_c(z) = v_m(x^{\mathrm{av}})(g_{\mathrm{EtOD}}/\mu_{\mathrm{EtOD}} + g_{\mathrm{D_2O}}/\mu_{\mathrm{D_2O}}),\end{aligned} \quad (24)$$

where V_c is the volume of the droplets per unit mass of gas mixture, and v_m is the molar volume of condensate in the droplet. This extrapolation assumes that the number of droplets per unit mass of gas mixture is constant, i.e., droplet formation and coagulation are negligible in the extrapolation region.

D. The effect of clustering

Small clusters in the gas phase will change both how we calculate the expected value of $\Delta h_{\mathrm{theor}}$ and how we interpret q. In particular, we measure the total monomer loss g_i from the gas phase, and yet monomer may be distributed between droplets, $g_{\mathrm{drop}\text{-}i}$, and clusters, $g_{cls\text{-}i}$, and, thus,

$$g_{\mathrm{drop}\text{-}i} = g_i - g_{cls\text{-}i}, \quad i = \mathrm{EtOD},\ \mathrm{D_2O}. \quad (25)$$

If $g_{cls\text{-}i}>0$ then the average composition of the droplets,

$$x^{\mathrm{av}} = \frac{g_{\mathrm{drop\text{-}EtOD}}/\mu_{\mathrm{EtOD}}}{g_{\mathrm{drop\text{-}EtOD}}/\mu_{\mathrm{EtOD}} + g_{\mathrm{drop\text{-}D2O}}/\mu_{\mathrm{D_2O}}}, \quad (26)$$

changes from that based solely on the measured g_i [Eq. (23)] and this directly affects the value of $\Delta h_{\mathrm{theor}}$. The partitioning between clusters and droplets also affects the values V_c in Eq. (24) and the number of droplets per unit mass of the gas mixture used in the energy balance [Eq. (B17) in Appendix B].

The measured q also consists of contributions from both droplet growth and cluster formation with

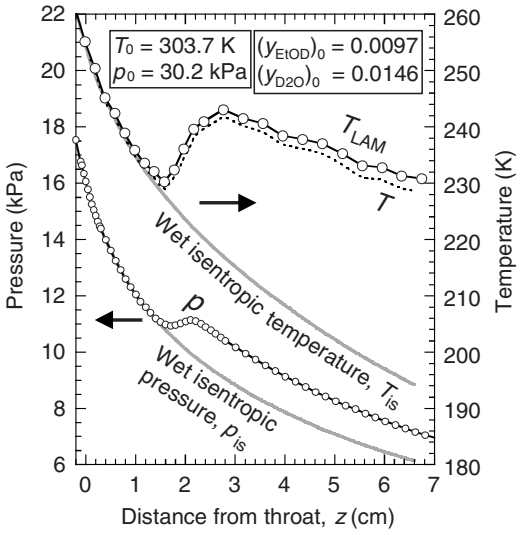

FIG. 2. Pressure p measured by PTM and temperature T_{LAM} by LAM in a condensing flow of EtOD/D_2O, which have already been shown in Ref. 4. T denotes the temperature at the center of the flow and is equivalent to T in the supersonic flow equations. T_{is} and p_{is} are the temperature and pressure in a fictitious flow, respectively, in which condensation or clustering does not occur. The mass fractions of EtOD and D_2O are 0.0166 and 0.0106, respectively.

$$q = q_{\text{drop}} + q_{cls}. \tag{27}$$

Thus, the experimental heat of dissociation of the droplets is

$$\Delta h_{\text{exp}} \equiv \frac{q_{\text{drop}}}{g_{\text{drop-EtOD}}/\mu_{\text{EtOD}} + g_{\text{drop-D}_2\text{O}}/\mu_{\text{D}_2\text{O}}}, \tag{28}$$

and this is the value that should agree with Δh_{theor} estimated by Eq. (22).

In the LAM, mole fractions of EtOD and D_2O monomer, y_i, are determined. The conversion between the y_i and g_i is given by Eq. (29) considering Eq. (5) and the relations, $\omega_{vi} = \omega_i - g_i$, $\omega_{cls} = g_{cls}$, and $\omega_c/\langle\mu_c\rangle \approx 0$.

$$y_i = \left(\frac{\omega_i - g_i}{\mu_{vi}}\right) \Bigg/ \left\{\frac{\omega_{\text{inert}}}{\mu_{\text{inert}}} + \sum_i \left(\frac{\omega_i - g_i}{\mu_{vi}}\right) + \frac{g_{cls}}{\langle\mu_{cls}\rangle}\right\}, \tag{29}$$

$$i = \text{EtOD},\ \ \text{D}_2\text{O}$$

where the contribution of the term $g_{cls}/\langle\mu_{cls}\rangle$ was estimated to be less than 0.1% under the conditions in this study, and therefore it was neglected throughout this study.

IV. RESULTS AND DISCUSSION

A. Pressure, temperature, and the concentrations of EtOD and D_2O monomers

Figure 2 illustrates the pressure profile measured by PTM and the temperature profile measured by LAM,[4] along with the temperature T at the center of the flow that was determined from T_{LAM}, after accounting for the presence of boundary layers as described in Sec. III B. When the pressure gradient dp/dz is positive, the boundary layer was assumed to be turbulent. Even if we assume that the boundary layer is laminar in this region, the estimated T only increases by 0.4 K, i.e., the uncertainty is less than our measurement uncertainty of ±1 K. T_{is} and p_{is} correspond to the fictitious expansion of a gas mixture with the same physical properties as of the condensing gas mixture but where neither condensation nor clustering occur. T_{is} and p_{is} are calculated using the supersonic flow Eqs. (9), (10), (20), and (12) by setting g and dg to zero, and using A/A^* derived from the p/p_0 measurements for a flow of pure carrier gas.[3] We determined the stagnation temperature T_0 by forcing T_{is} to agree with T near the throat, z=0.1–1.0 cm, where neither condensation nor clustering occur, and found that T_0=30.5 °C (303.7 K).

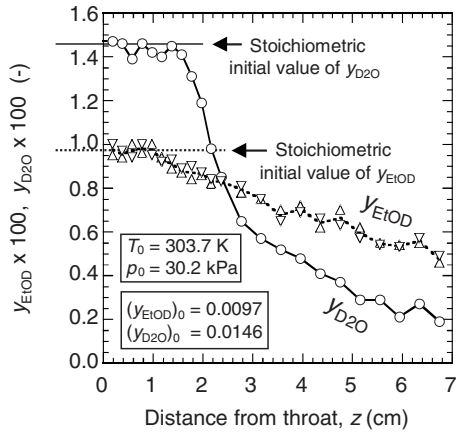

FIG. 3. Mole fractions of EtOD and D_2O monomers measured by LAM, y_{EtOD} and $y_{\text{D}_2\text{O}}$, which have already been shown in Ref. 4.

The mole fractions of EtOD and D_2O monomer, measured by LAM,[4] are shown in Fig. 3. Two independent y_{EtOD} measurements were made at each position and both show that y_{EtOD} starts to decrease monotonically at z=1.0 cm. In contrast $y_{\text{D}_2\text{O}}$ does not start to decrease monotonically until ~0.4 cm further downstream at z=1.4 cm. Upstream of this point, the measured $y_{\text{D}_2\text{O}}$ values fluctuate below the stoichiometric initial value. Similar fluctuations were observed upstream of the throat, too, though those are not shown in the figure. These fluctuations are not clearly correlated with a detectable increase in pressure as will be shown in Fig. 4. They are, therefore, not likely due to condensation or formation of stable clusters. Instead, those fluctuations may be related to the formation of unstable clusters or to a measure-

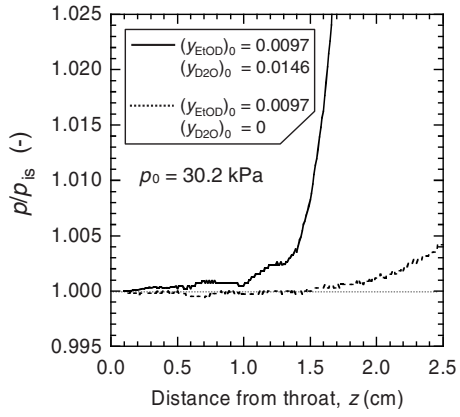

FIG. 4. Pressure ratio p/p_{is} in the EtOD/D_2O flow and pure EtOD flow. T_0 is estimated to be 303.7 K in the EtOD/D_2O flow, and 303.2–306.2 K in the pure EtOD flow. See text for discussion about the correction for temperature difference between the two PTM.

ment error. Nevertheless, a small amount of continuous depletion of D_2O monomer cannot be denied in this region.

This amount is estimated to be much smaller than the depletion of EtOD as follows. The measured values of y_{D_2O} are not expected to exceed the actual value, because the measured values of y_{D_2O} around the throat do not exceed the stoichiometric initial value, $(y_{D_2O})_0$. Therefore, the decrease in the actual value of y_{D_2O} from $(y_{D_2O})_0$ at $z=1.4$ cm is expected to be less than or equal to the decrease (0.0001) in the measured y_{D_2O} value at this position. This is only about 15% of the decrease in the measured value of y_{EtOD} at the same position. As a result, we conclude that the onset point of phase change (condensation or clustering) of EtOD is $z=1.0$ cm and that of D_2O is $z=1.4$ cm. Based on the maximum deviations from the stoichiometric initial values around the throat, we estimate the error in y_{EtOD} is $\pm 2\%$ and that in y_{D_2O} is $(-2\pm 2)\%$.

If we examine the initial deviation of p from p_{is} more closely in the EtOD/D_2O flow, we observe, as shown in Fig. 4 by the solid line, that there is a distinct and systematic increase, which starts at $z=1.0$ cm, and p/p_{is} reaches 1.001, at $z=1.1$ cm. Since a 0.1% deviation in p from p_{is} is the smallest change we can reliably detect, we ignore pressure deviations where $|p/p_{is}-1|<0.001$ and define the onset position of the deviation of p from p_{is}, z_{on_p}, as the position where p/p_{is} reaches 1.001. Comparing Figs. 3 and 4, we see that the initial, rather gentle, pressure increase corresponds closely to the decrease in y_{EtOD} that starts near $z=1.0$ cm, while the rapid increase in p/p_{is} at $z>1.4$ cm is related to the rapid decrease in y_{D_2O}. In contrast, there is no clear correlation between the fluctuations in y_{D_2O} and p/p_{is} at $z\leq 1.4$ cm. As discussed above, the pressure increase at $z=1.0-1.4$ cm is primarily due to the heat release from either condensation or clustering of EtOD although we acknowledge that a small amount of D_2O may associate with EtOD to form EtOD/D_2O clusters or droplets.

To determine whether a pure EtOD flow (N_2+CH_4+EtOD) undergoes condensation or clustering under similar conditions, we made a PTM for pure EtOD at the same p_0, $(y_{EtOD})_0$, and the same nominal value of T_0. As illustrated by a dashed line in Fig. 4, for the pure EtOD experiment the onset position z_{on_p} is 2.1 cm, or ~1.0 cm further downstream than for the EtOD/D_2O flow. Even if we account for the fact that T_0 may differ between the two experiments, for reasons detailed in our previous paper,[4] we estimate that for the EtOD flow z_{on_p} is at least 1.7 cm, that is 0.6 cm further downstream from that observed for the EtOD/D_2O flow, 1.1 cm, and that the temperature and the partial pressure of EtOD in the EtOD/D_2O flow do not reach the conditions required for condensation and/or clustering of pure EtOD to occur (Appendix E). Thus, it is clear that the condensation and/or clustering of EtOD is promoted by the presence of D_2O.

Likewise, the onset position z_{on_p} for pure D_2O flow, at the same temperature and the partial pressure of D_2O used in the EtOD/D_2O experiment, was determined to be 2.9 cm using the same method as for pure EtOD flow (Appendix E).

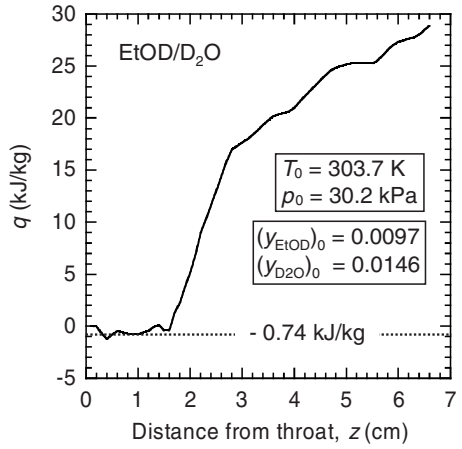

FIG. 5. Latent heat released in a unit mass of gas mixture, q, which was derived from the PTM and LAM measurements using supersonic flow equations, Eqs. (9)–(12).

In this case there is no uncertainty in T_0, because the results of the PTM of pure D_2O condensation at well defined T_0(=25.0 °C)[3] were available.

B. Latent heat released in EtOD/D_2O flow

In the previous section, we detected the heat release to the flow qualitatively based on the deviation of the pressure from the isentropic value. In this section, we determine q quantitatively using the procedures described in Sec III A.

Figure 5 shows the variation of q as a function of position determined by integrating Eqs. (9)–(12) from our usual starting position, $z=0.1$ cm. Near $z=1.0$ cm, where p starts to deviate from p_{is} and y_{EtOD} starts to decrease, $q=-0.74$ kJ/kg. This small, negative deviation is caused by the deviation of the condensing flow temperature T at $z=0.1$ cm from the isentropic temperature T_{is} by 0.6 K. Since T and T_{is} agree further downstream, the integration yields a small negative value for q up to the point of true heat addition. To avoid this artifact, we added 0.74 kJ/kg to the value of q in the remaining analysis.

As illustrated in Fig. 5, q increases slowly between $z=1$ and $z=1.6$ cm, before increasing rapidly as D_2O begins to condense. In contrast, as shown in Fig. 4, p/p_{is} starts to increase rapidly 0.2 cm further upstream at $z=1.4$ cm. The start of the rapid increase in p at $z=1.4$ cm is due to a decrease in A/A^*, where A/A^* was also determined using Eqs. (9)–(12). As Matsuo *et al.*[15] and we[3] reported for water condensation (H_2O or D_2O), the thickness of the boundary layer on the wall of the nozzle first increases relative to the value in the isentropic expansion a few millimeters upstream of the start of condensation before decreasing further downstream. As the boundary layer thickness increases, A/A^* decreases relative to the isentropic value. Thus, p/p_{is} increases because p decreases more slowly in the nozzle with the lower effective expansion rate.

We next compare, in Fig. 6, the experimental molar heat of dissociation, Δh_{exp}, with Δh_{theor} assuming that clustering does not occur, i.e., $g_{cls\text{-EtOD}}=g_{cls\text{-}D_2O}=0$ and $q_{cls}=0$ [see Eqs. (25) and (27)]. Figure 6(a) shows the mole fractions of EtOD in the droplet, x^{av}, x^b, and x^s, values that are required in order

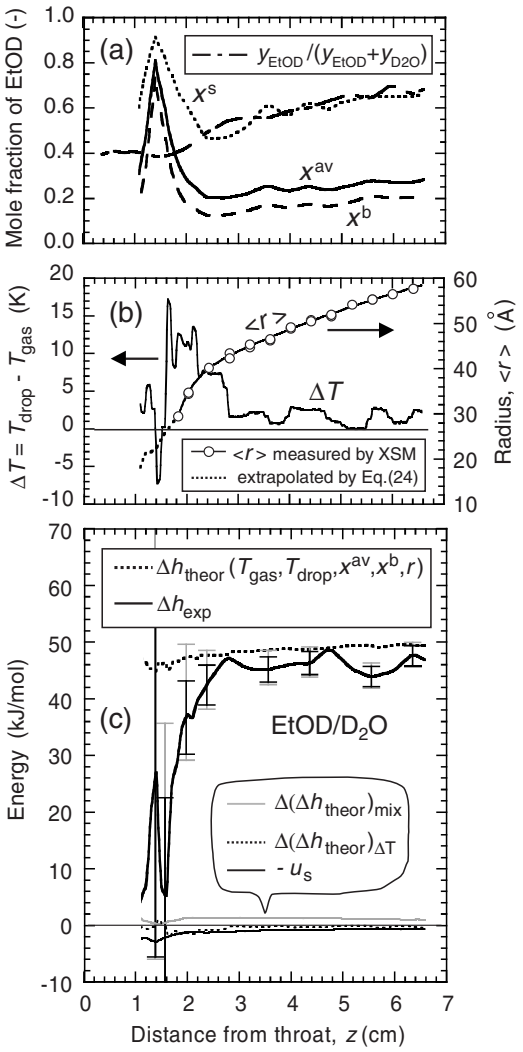

FIG. 6. Results of the determination of molar latent heat in the EtOD/D_2O condensing flow, Δh_{exp} and Δh_{theor}. The former was determined experimentally using the supersonic flow equations and the latter was estimated from the thermodynamic properties of EtOD/D_2O mixtures, and both were obtained on the assumption that clustering does not occur. (a) Mole fractions of EtOD in the EtOD/D_2O droplet, average mole fraction, x^{av}, bulk mole fraction, x^b, and surface mole fraction, x^s, these were calculated in the determination process of Δh_{theor}. Mole fraction ratio in vapor phase, $y_{EtOD}/(y_{EtOD}+y_{D2O})$, is also shown. (b) Difference of the temperatures between the EtOD/D_2O droplet and gas, ΔT and the average radius of the droplet, $\langle r \rangle$. The extrapolated line of $\langle r \rangle$ (dotted line) and ΔT were calculated in the determination process of Δh_{theor}. (c) Comparison between Δh_{exp} and Δh_{theor}. The contribution of surface energy on Δh_{theor}, $-u_s$, is also shown as well as the contribution of mixing enthalpy, $\Delta(\Delta h_{theor})_{mix}$, and that of ΔT, $\Delta(\Delta h_{theor})_{\Delta T}$.

to determine Δh_{theor}, as well as the relative mole fraction of EtOD in the vapor phase, $y_{EtOD}/(y_{EtOD}+y_{D_2O})$. Figure 6(b) shows the droplet radius $\langle r(z) \rangle$ and the temperature difference between the droplet and vapor, $\Delta T = T_{drop} - T_{gas}$. Finally, based on the results in Figs. 6(a) and 6(b), we determined Δh_{theor}, and compared it with Δh_{exp} in Fig. 6(c). The contributions to Δh_{theor} due to the mixing enthalpy, surface energy, and the temperature difference between the droplet and gas, that is, $\Delta(\Delta h_{theor})_{mix}$, $-u_s$, and $\Delta(\Delta h_{theor})_{\Delta T}$, are also shown in Fig. 6(c), and all are clearly much smaller than the energy release due to condensation of the pure components. For selected values of Δh_{exp} the black error bars represent the uncertainty caused by an error of ± 1 K in the LAM temperature measurements, while the gray bars include the additional uncertainty that stems from the error in the mole fractions of EtOD and D_2O. Furthermore, the gray error bars are calculated so that the uncertainties introduced by errors in temperature and mole fraction have the same sign. Since these two errors may cancel in some cases, the gray bars represent the largest error we expect for Δh_{exp}. Although measurement uncertainties also affect the calculated values of Δh_{theor} the changes are only 1.7 and 0.6 kJ/mol at $z=1.4$ and 1.6 cm, respectively, and less than 0.3 kJ/mol at $z>1.8$ cm, and these error bars are, therefore, omitted.

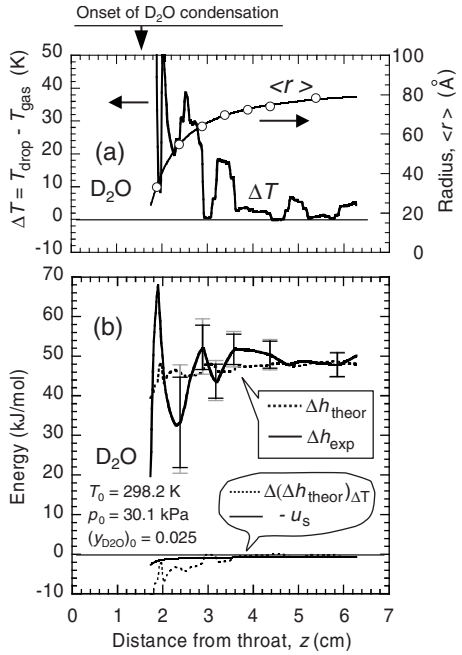

FIG. 7. Results of the determination of molar latent heat in the D_2O condensing flow, Δh_{exp} and Δh_{theor}. The former was determined experimentally using the supersonic flow equations and the latter was estimated from the thermodynamic properties of D_2O, and both were obtained on the assumption that clustering does not occur. (a) Difference of the temperatures between the D_2O droplet and gas, ΔT, and the average radius of the droplet, $\langle r \rangle$. ΔT was calculated in the determination process of Δh_{theor}. (b) Comparison between Δh_{exp} and Δh_{theor}. The contribution of surface energy on Δh_{theor}, $-u_s$, is also shown as well as the contribution of ΔT, $\Delta(\Delta h_{theor})_{\Delta T}$. The definition of the error bars is the same as those in Fig. 6(c) except that the uncertainty in T_{LAM} (y_{D_2O}) is not ± 1 K ($-2 \pm 2\%$) but ± 2 K ($\pm 2\%$).

As shown in Fig. 6(c), Δh_{exp} is generally lower than Δh_{theor}, and especially low around the onset point of condensation ($z=1.6$ cm). The Δh_{exp} increases rapidly with the progress of condensation between the onset point and $z=\sim 2.5$ cm, and even at $z>2.5$ cm, Δh_{exp} is on average lower than Δh_{theor} by 2.8 kJ/mol. We expect that the droplets formed in the nozzle are spherical, and indeed the x-ray spectra (intensity versus momentum transfer) are only fit well by a polydisperse distribution of spherical droplets. The low value of Δh_{exp} cannot, therefore, be attributed to any abnormal droplet structure.

To emphasize that the difference between Δh_{exp} and Δh_{theor} is unlikely due to any identified experimental or estimation error, we applied the same analysis method to our earlier D_2O condensation data.[3] The results are shown in Fig. 7. The temperature difference and droplet radii are shown in

Fig. 7(a), where the radii were estimated from SAXS measurements (Appendix F). As shown in Fig. 7(b), although there are fluctuations around the expected value of Δh_{theor}, due in part to the less accurate and less well resolved temperature measurements (± 2 K, $\Delta z=0.2-0.6$ cm), when $z>2.5$ cm, Δh_{exp} agrees on average with Δh_{theor} with a error of +1.1 kJ/mol. The agreement is especially good when $z \geq 4.4$ cm, a region where the temperature decreases linearly with distance and the analysis does not suffer from the lack of resolution in the temperature measurement. Furthermore, although it is not shown here, we obtained similar good agreement when $(y_{D_2O})_0=0.017$. This suggests that the methods used to determine Δh_{exp} and the heat of vaporization $\Delta h_{\text{vap-D}_2\text{O}}^{\text{bulk/pure}}$ in Eq. (B11) are appropriate. Finally, in order to explain the difference between Δh_{exp} and Δh_{theor}, observed in Fig. 6(c) when $z>2.5$ cm, by an error in the estimation of $\Delta h_{\text{vap-EtOD}}^{\text{bulk/pure}}$, this value would have to be overestimated by 24%, and it is unlikely that this error is so large.

One possible reason for the low value of Δh_{exp} observed during EtOD/D_2O condensation is the presence of small clusters in the gas phase, that is, g_{cls} is not zero although $g_{cls}=0$ was assumed to derive the results in Fig. 6. As shown in Fig. 6(c), Δh_{exp} only starts to increase rapidly at $z=1.6$ cm. Hence, for $z \leq 1.6$ cm, the depletion of EtOD and D_2O monomer is expected to be due to the formation of clusters.

C. Sizes of clusters upstream of the onset point of condensation

Generally, the size of the cluster can be estimated from the size dependent heat of dissociation. However, the values of the heat of dissociation shown in Fig. 6(c) include large errors at $z \leq 1.6$ cm. Therefore, in this study, we estimate the cluster size from the PTM without using the measurements of T_{LAM}. This estimate should be more accurate than that from the heat of dissociation because the error of the pressure measurement is about 0.1%, while that of the temperature measurement is about 0.5%.

As described in Sec. IV A, the pressure at $z \geq 1.4$ cm is affected by condensation, and therefore, the cluster size is estimated from PTM in the region $z=1.0-1.4$ cm. Furthermore, in this region, the fluctuations of y_{D_2O} at $z<1.4$ cm have no effect on the pressure. Hence, the pressure profile in this region can be analyzed in the same way as for the single-component (EtOD) condensation. Though we do not deny the possibility that a small amount of D_2O associates with EtOD to form EtOD/D_2O clusters or droplets, this effect on the PTM should be negligible.

For single-component condensation, when p/p_0, A/A^*, and L are given, g can be derived by using the supersonic flow equations, Eqs. (9), (10), (20), and (12).[3] By applying this method to the clustering of EtOD, and comparing the derived g_{EtOD} (termed $g_{\text{EtOD-PTM}}$) to the g_{EtOD} measured by LAM, $g_{\text{EtOD-LAM}}$, we can estimate the size of the clusters as follows.

When Eq. (20) is applied to the clustering of EtOD, the heat of dissociation of the cluster should be used for L instead of the heat of vaporization of the bulk liquid, and in Eq. (19) the isobaric heat capacity of the EtOD cluster should be used for $c_{p(l)}$ to evaluate c_p. Since, however, g_{EtOD} at $z=1.4$ cm is only 0.0011, $c_{p(l)}=c_{p\text{-EtOD}(v)}$ was assumed for simplicity. This assumption is equivalent to assuming that the heat of dissociation of the cluster is independent of the temperature, because $\partial L/\partial T=c_{p(v)}-c_{p(l)}$, and the temperature-independent heat of dissociation of the cluster was successfully assumed in the analyses of the temperature and pressure dependencies of the isobaric heat capacity of ethanol vapor.[16,17]

A/A^* is also required to derive g_{PTM}. In a condensing flow (wet flow), $(A/A^*)_{\text{Wet}}$ is affected by the condensation process.[3] As described in the Sec. IV B, $(A/A^*)_{\text{Wet}}$ decreases compared to the value observed for the noncondensing flow (dry flow), $(A/A^*)_{\text{Dry}}$, when p starts to deviate from p_{is}. In order to estimate the effect of the change in A/A^* on the calculated value of g_{PTM}, the fractional change, $fcg_{\text{PTM}} \equiv \{g_{\text{PTM}} \text{ with } (A/A^*)_{\text{Dry}}\}/\{g_{\text{PTM}} \text{ with } (A/A^*)_{\text{Wet}}\}-1$, was determined for the two measurements in our previous study[3] of D_2O condensation. The D_2O studies used the same nozzle as the current work and the stagnation conditions were $T_0=298.2$ K, $p_0=30.1$ kPa, and $(y_{D_2O})_0=0.017$ and 0.025. By analyzing our previous experiments, we found that we could correlate the maximum value of fcg_{PTM} with the maximum value of $d(p-p_{\text{is}})/dz$ and that $(fcg_{\text{PTM}})_{\max}=[a\{d(p-p_{\text{is}})/dz\}_{\max}]^b$, where $a=0.50$ cm/kPa and $b=2.8$, respectively. In the current study, in the region $z=1.0-1.4$ cm, $\{d(p-p_{\text{is}})/dz\}_{\max}$ was 0.10 kPa/cm, and therefore, $(fcg_{\text{PTM}})_{\max}$ was estimated to be only 2.3×10^{-4}. It is therefore safe to assume $A/A^*=(A/A^*)_{\text{Dry}}$ in this calculation, where $(A/A^*)_{\text{Dry}}$ can be obtained from the PTM of the dry flow.[3]

We next considered the effect of $\omega_{cls}/\langle\mu_{cls}\rangle$ in Eq. (5) on determining Δh_{exp} and g_{PTM}. As described in Sec. III A, the flow equations in this study, Eqs. (9)–(12), and those in the previous study,[3] Eqs. (9), (10), (20), and (12), are based on the basic equations, Eqs. (2)–(5). In both cases, the number density of the clusters, $\omega_{cls}/\langle\mu_{cls}\rangle$ in Eq. (5) was neglected as well as $\omega_c/\langle\mu_c\rangle$. This should be a good approximation when only condensation occurs and significant clustering does not. In the EtOD/D_2O condensing flow in this study, EtOD-dominant clusters are expected to form in the nozzle, and, as will be shown in Sec. IV D, the mass fraction of clusters was estimated to be about 0.002 for $z \geq 1.6$ cm. In order to investigate how $\omega_{cls}/\langle\mu_{cls}\rangle$ affects Δh_{exp}, we used the value for the dimer, $0.002/(2\mu_{\text{EtOD}})$, and estimated the change from the values presented in Fig. 6(c). We found that Δh_{exp} increased by 2% at $z=1.6$ cm and by less than 0.2% at $z \geq 2.0$ cm. These changes are negligibly small and neglecting $\omega_{cls}/\langle\mu_{cls}\rangle$ in Eq. (5) does not affect the value of Δh_{exp} in spite of the formation of EtOD clusters.

When, however, g_{PTM} for the clusters is determined from the pressure measurements, the effect of $\omega_{cls}/\langle\mu_{cls}\rangle$ cannot be neglected, because $\omega_{cls}/\langle\mu_{cls}\rangle$ directly affects the pressure as expressed in Eq. (5), and the heat of dissociation of the cluster is much smaller than the heat of vaporization. Since the increase in the pressure caused by the latent heat release from the cluster is very small, any error in the pressure af-

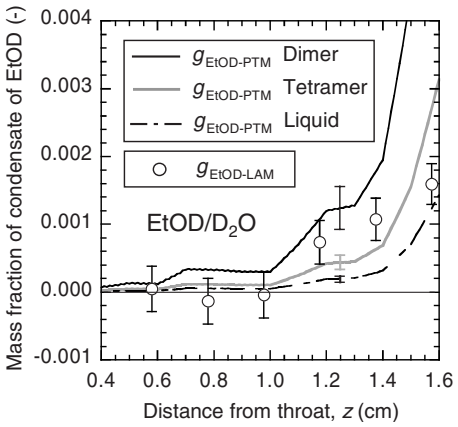

FIG. 8. Comparison of the mass fractions of the condensate of EtOD, $g_{\mathrm{EtOD\text{-}PTM}}$ and $g_{\mathrm{EtOD\text{-}LAM}}$, where $g_{\mathrm{EtOD\text{-}PTM}}$ was determined from the PTM assuming EtOD forms dimer or tetramer, and $g_{\mathrm{EtOD\text{-}LAM}}$ was measured by LAM. The $g_{\mathrm{EtOD\text{-}PTM}}$ estimated assuming EtOD bulk liquid condense is also shown for reference (alternative long and short dash line).

fects the accuracy of g_{PTM} significantly. Hence, in this section, $\omega_{cls}/\langle\mu_{cls}\rangle$ is expressed by Eq. (30) assuming that only EtOD clusters are formed at $z \leq 1.4$ cm.

$$\frac{\omega_{cls}}{\langle\mu_{cls}\rangle} = \frac{g_{\mathrm{EtOD\text{-}PTM}}}{n_{c\_\mathrm{EtOD}}\mu_{\mathrm{EtOD}}}, \tag{30}$$

where n_{c_EtOD} is the number of EtOD molecules in a cluster. To be consistent with the change in Eq. (5), Eqs. (14) and (15) are replaced by Eqs. (31) and (32), respectively.

$$w_0(g) \equiv \frac{\mu}{\mu_0\{1-(1-1/n_{c\_\mathrm{EtOD}})g_{\mathrm{EtOD\text{-}PTM}}\}}, \tag{31}$$

$$w(g) \equiv \frac{\mu(1-1/n_{c\_\mathrm{EtOD}})}{\mu_{\mathrm{EtOD}}\{1-(1-1/n_{c\_\mathrm{EtOD}})g_{\mathrm{EtOD\text{-}PTM}}\}}. \tag{32}$$

We then determined $g_{\mathrm{EtOD\text{-}PTM}}$ assuming that the clusters are all dimers or all tetramers, and compared these values with $g_{\mathrm{EtOD\text{-}LAM}}$. The values of L for EtOD clusters, $L_{cls\text{-}\mathrm{EtOD}}$, were estimated assuming that the molar heats of dissociation of EtOD clusters are the same as those of EtOH,[13] i.e., $\Delta h_{\mathrm{dis\_EtOD(2)}}=9.92$ kJ/(mol monomer) for the dimer and $\Delta h_{\mathrm{dis\_EtOD(4)}}=23.42$ kJ/(mol monomer) for the tetramer. Thus, we have

$$L_{cls\text{-}\mathrm{EtOD}} = \Delta h_{\mathrm{dis\_EtOD(2)}}/\mu_{\mathrm{EtOD}} = 210.7 \text{ kJ/kg for the dimer}, \tag{33}$$

$$L_{cls\text{-}\mathrm{EtOD}} = \Delta h_{\mathrm{dis\_EtOD(4)}}/\mu_{\mathrm{EtOD}} = 497.6 \text{ kJ/kg for the tetramer}. \tag{34}$$

Furthermore, we determined $g_{\mathrm{EtOD\text{-}PTM}}$ on the assumption that the condensate is the bulk EtOD liquid by using the heat of vaporization of the pure EtOD liquid for L and neglecting $\omega_{cls}/\langle\mu_{cls}\rangle$.

In Fig. 8, the values of $g_{\mathrm{EtOD\text{-}PTM}}$ (solid lines for clusters and an alternating long and short dashed line for liquid) are compared with $g_{\mathrm{EtOD\text{-}LAM}}$ measured by LAM (open circles). The error bars of the $g_{\mathrm{EtOD\text{-}LAM}}$ represent the uncertainty caused by an error of $\pm 2\%$ in the LAM measurements of y_{EtOD}. The error bars of the $g_{\mathrm{EtOD\text{-}PTM}}$, which correspond to the error of $\pm 0.1\%$ in the pressure measurements, are shown only at $z=1.25$ cm for good viewability. At $z=1.0-1.4$ cm, the $g_{\mathrm{EtOD\text{-}LAM}}$ generally lies between the lines of $g_{\mathrm{EtOD\text{-}PTM}}$ for the dimer and tetramer. When $z>1.4$ cm, the comparison is no longer valid because $g_{\mathrm{EtOD\text{-}PTM}}$ is affected by changes in A/A^* due to the onset of condensation as discussed in Sec. IV B. The EtOD-dominant clusters in the region $z=1.0-1.4$ cm are, therefore, expected to range from dimers to tetramers. The main species of the small EtOD-dominant clusters should be the small pure EtOD clusters, because the average number of D_2O molecules in a cluster is much less than unity.

TABLE I. Equilibrium constants, K_2 and K_4, at 298.15 K for cluster formation and the heats of dissociation of the clusters, $\Delta H_{\mathrm{dis\_2}}$ and $\Delta H_{\mathrm{dis\_4}}$.

	Dimer		Tetramer	
	K_2 (298.15 K) ($\mathrm{MPa^{-1}}$)	$\Delta H_{\mathrm{dis\_2}}$ (kJ/mol)	K_4 (298.15 K) ($\mathrm{MPa^{-3}}$)	$\Delta H_{\mathrm{dis\_4}}$ (kJ/mol)
	$(EtOH)_2$		$(EtOH)_4$	
Massucci *et al.*[a]	0.8247	19.84	1206	93.68
Barrow *et al.*[b]	0.73	14.2	2320	103.7
Counsell *et al.*[c]	0.94	15.8	1736	101.85
Current work[d]	$(EtOH)_2$			
	0.86	15.0		
	$(H_2O)_2$			
	0.50	14.4		
	$(EtOH)(H_2O)$			
	1.19	14.1		

[a]Reference 13.
[b]Reference 16.
[c]Reference 17.
[d]These values were determined from the second virial coefficients of $EtOH/H_2O$ mixture vapor as described in Appendix G.

D. Expected equilibrium cluster concentrations at $z=1.4$ cm

To determine whether or not the concentrations of small clusters estimated above are consistent with those of a vapor in chemical equilibrium, we first calculated the equilibrium concentrations of pure EtOD, pure D_2O, and mixed $EtOD/D_2O$ clusters (dimers/tetramers) using the temperatures and partial pressures of EtOD and D_2O found in the $EtOD/D_2O$ nozzle experiments at $z=1.4$ cm. All calculations assume that the differences between EtOD (D_2O) and EtOH (H_2O) are negligible, because the difference between those molecules is only the mass of the hydrogen, and, according to the thermodynamic properties in Appendix C, the heat of vaporization of EtOD (D_2O) is only about 2% (4%) higher than that of EtOH (H_2O) in the temperature range of this study, 225–260 K. Table I summarizes the thermodynamic data used in the calculations.

If we use the most recent data of Massucci *et al.*,[13] we find that the equilibrium fraction of EtOD contained in pure dimers and tetramers is only 0.0019. The fractional depletion of EtOD derived experimentally from the decrease in y_{EtOD} shown in Fig. 3 is 0.06. Thus, the equilibrium dimer and

tetramer concentrations represent only 3% of the total EtOD depletion. Furthermore, this calculated result is consistent with our discussion of Fig. 4 in Sec. IV A where we noted that clustering or condensation of EtOD begins to occur for $z \leq 1.4$ cm in the nozzle only because of the presence of D_2O.

We then estimated the equilibrium constants and the heats of dissociation of the pure and mixed dimers, $(EtOH)_2$, $(EtOH)(H_2O)$, and $(H_2O)_2$, from the second virial coefficients of $EtOH/H_2O$ mixtures measured by Noppe *et al.*[18] (see Appendix G). Although our parameters for $(EtOH)_2$ are slightly different from those of Massucci *et al.* as shown in Table I, they are within the range of values reported in the literature, and the relative concentrations of the three dimer types should be reasonable.

Let [species] denote the number density of a given species. Then using our parameters, we estimate that [EtOD in $(EtOD)_2$]/[EtOD]=0.0009, [EtOD in $(EtOD)(D_2O)$]/[EtOD]=0.0009, and [D_2O in $(D_2O)_2$]/[D_2O]=0.0008; i.e., the amount of EtOD in the heterodimer $(EtOD)(D_2O)$ should be similar to that in the pure dimer $(EtOD)_2$ if the clusters are in the equilibrium state. Furthermore, according to a quantum density functional calculation with the B3LYP hybrid functional and the 6-31+G(d) basis set, the binding energy of the heterotrimer $(EtOH)_2(H_2O)$, 49.1 kJ/mol, is similar to that of the pure trimer $(EtOH)_3$, 51.0 kJ/mol.[19] Thus, it is unlikely that the equilibrium constants of the heteroclusters of EtOD and D_2O are much larger than those of the pure EtOD clusters when $n \leq 4$. At $z < 1.4$ cm, the equilibrium concentrations of the clusters are smaller than those at $z=1.4$ cm due to the higher temperature. In summary, the depletion of the EtOD monomer at $z=1.4$ cm, and further upstream, cannot be explained by equilibrium cluster concentrations in the vapor.

E. A possible mechanism for the formation of EtOD clusters

The evidence presented in Secs. IV A–IV D shows that in the region $z=1.0-1.4$ cm the formation of small (dimer-tetramer) clusters, predominantly containing EtOD, is facilitated by the presence of D_2O and that the depletion of the EtOD monomer is much larger than expected based on monomer-dimer-tetramer equilibrium. This suggests that there is an alternate route to produce small EtOD clusters. One possible mechanism is given by Eq. (35).

$$n(\mathrm{EtOD}) + (\mathrm{EtOD})_i(\mathrm{D_2O})_j \rightarrow (\mathrm{EtOD})_n + (\mathrm{EtOD})_i(\mathrm{D_2O})_j, \quad i \geq 1 \;\; j \geq 1, \quad n = 2 \sim 4, \tag{35}$$

where the mixed clusters $(EtOD)_i(D_2O)_j$ facilitate the formation process, i.e., the EtOD monomers are absorbed into the $EtOD/D_2O$ cluster and pure $(EtOD)_n$ clusters evaporate from the mixed cluster. The depletion of D_2O monomer in this region of the nozzle is not as large as that of EtOD, and so we infer that the concentration of $EtOD/D_2O$ clusters is much smaller than that of pure $(EtOD)_n$ clusters. Since the role of the $EtOD/D_2O$ clusters is to absorb energy and facilitate pure EtOD cluster formation, larger $EtOD/D_2O$ clusters are expected to be more effective. The biggest $EtOD/D_2O$ clusters in the nozzle are the droplets produced by condensation. Thus, the low value of Δh_{exp} shown in Fig. 6(c) may be due to EtOD clusters produced by the mechanism expressed by Eq. (35), not only in the region $z=1.0-1.4$ cm, but also further downstream. This hypothesis can explain the observations downstream of the onset of condensation as follows.

The molar concentrations of EtOD and D_2O monomers, derived from the temperature and pressure in Fig. 2 and the mole fractions in Fig. 3, both decrease monotonically except for the small fluctuations. If clusters are formed in the vapor phase, they should disappear when $z=2.0-4.9$ cm, because, as shown in Fig. 2, in this region the temperature is higher than the value ($T=234.7$ K) found at $z=1.0$ cm where EtOD-dominant clusters start to form. The difference between Δh_{exp} and $\Delta h_{\mathrm{theor}}$ shown in Fig. 6(c), however, suggests that detectable levels of clusters persist in the region $z=2.0-4.9$ cm. Downstream of the onset point of condensation, clusters may, therefore, be formed in $EtOD/D_2O$ droplets and evaporate from them. The cluster compositions cannot be determined in this region differently for $z=1.0-1.4$ cm. However, pure EtOD clusters are expected to be predominantly produced downstream of the onset of condensation as well as for $z=1.0-1.4$ cm. As detailed below, pure EtOD clusters may evaporate from the $EtOD/D_2O$ droplets when the EtOD concentration in the droplets exceeds a certain level. Since the mole fraction ratio, $y_{\mathrm{EtOD}}/(y_{\mathrm{EtOD}}+y_{\mathrm{D_2O}})$, is higher downstream of the onset than upstream [Fig. 6(a)], the concentration of EtOD in the droplets should also be increasing.

Our hypothesis is motivated by the experiments of Nishi *et al.*,[8] and Wakisaka and Ohki[9] who analyzed the mass spectra of clusters generated through the adiabatic expansion of mists formed from $EtOH/H_2O$ solutions. They found that the self-association of EtOH is promoted by the presence of H_2O, that is, in the expansion of a pure EtOH mist, the intensities of the pure EtOH clusters are lower than in the expansion of mists formed from $EtOH/H_2O$ mixtures, especially for clusters containing more than three ethanol molecules. Furthermore, pure EtOH clusters were the predominant species in the small clusters, $(EtOH)_n(H_2O)_m$ $n \leq 7$, when the mole fraction of EtOH in the solution was larger than 0.12 (Fig. 4 in Ref. 8, Fig. 3 in Ref. 9). In those experiments, the partial pressures of EtOH and H_2O in vapor phase are negligibly small compared to those in our nozzle, and, in contrast with what occurs during condensation in the nozzle, collisions between the droplets and the monomer are very rare. A quantitative comparison between the results of the mass spectrometry and LAM in the nozzle is, therefore, not possible. Furthermore, the effect of droplet size on the formation of EtOH clusters was not investigated in those studies, and, thus, it is not known how the small heterogeneous clusters help to form EtOH clusters. Nevertheless, qualitatively, the mass spectroscopy results support our hypothesis that small pure EtOD clusters (dimer-tetramer) predominantly evaporate from $EtOD/D_2O$ particles.

There is another interesting phenomena observed by Sato *et al.*, which may support our hypothesis. They atom-

ized EtOH/H_2O solutions by using an ultrasonic vibrator at a frequency of 2.3 MHz and measured the ethanol concentration of the mist thus produced.[20] They found that the ethanol concentration increased as the solution temperature decreased and pure ethanol was detected at 10 °C even when the ethanol mole fraction in the solution was around 0.1. The size of the ethanol-rich mist particles was determined to be about ten molecules by SAXS measurement.[21] Though the role of the ultrasonic vibration is not clear, these observations, together with the mass spectroscopy results, encourage us to consider our hypothesis [Eq. (35)] in more detail.

According to our hypothesis, we can estimate $g_{cls\text{-EtOD}}$ downstream of the onset point of condensation ($z>1.6$ cm) by forcing Δh_{exp} to agree with Δh_{theor} assuming $g_{cls\text{-}D_2O}=0$. The EtOD clusters were assumed to be either dimers or tetramers, and $L_{cls\text{-EtOD}}$ in Eq. (33) or Eq. (34) was used to determine the value of $q_{cls}=g_{cls\text{-EtOD}}L_{cls\text{-EtOD}}$. The results for these two cases are shown in Fig. 9. In Fig. 9(a), the mole fraction ratio of EtOD monomer in the vapor phase, and the mole fractions of EtOD in the droplet are shown. Generally speaking, all those values increase as the droplets grow. The temperature differences between the droplet and gas, shown in Fig. 9(b), decrease monotonically with the droplet growth except for small fluctuations.

The values of $g_{cls\text{-EtOD}}$ are shown in Fig. 9(c). The line of $g_{cls\text{-EtOD}}$ for the dimer (tetramer) is not shown when $z<1.9$ cm (2.4 cm) because q is too small and the determined value of $g_{cls\text{-EtOD}}$ exceeds that of g_{EtOD}. The error bars of $g_{cls\text{-EtOD}}$ are shown only for the case of dimers. The error for $g_{cls\text{-EtOD}}$ of tetramers is about 1.5 times larger than that for dimers. An error bar for g_{EtOD} is shown at $z=1.6$ cm to emphasize that for $z\leq 1.6$ cm we expect $g_{cls\text{-EtOD}}=g_{\text{EtOD}}$ as discussed in Sec. IV B. As shown in Fig. 9(c), $g_{cls\text{-EtOD}}$ for tetramers is larger than that for dimers. This is because $L_{cls\text{-EtOD}}$ of the tetramer (497.6 kJ/kg) is larger than that of the dimer (210.7 kJ/kg). The averaged value of $g_{cls\text{-EtOD}}$ is 0.0018 (0.0027) for the case of the dimer (tetramer), which corresponds to 11% (16%) of the total EtOD molecules. Although we do not have enough data to determine the size of EtOD clusters downstream of the onset of condensation, we can conclude that, on average, at least ~10% of EtOD molecules form clusters downstream of the onset point of condensation.

Finally, we consider the possibility that the small EtOD clusters exist at much higher concentration than in the equilibrium state. Here the discussion is restricted to the formation of EtOD dimer. The mechanism of the dimer formation in the vapor phase is expressed by Eqs. (36) and (37).[22]

$$\mathrm{A}+\mathrm{A}\underset{k_2}{\overset{k_1}{\rightleftarrows}}\mathrm{A}_2^*, \tag{36}$$

$$\mathrm{A}_2^*+\mathrm{M}\underset{k_4}{\overset{k_3}{\rightleftarrows}}\mathrm{A}_2+\mathrm{M}, \tag{37}$$

where A and A_2 are the EtOD monomer and dimer, respectively. A_2^* denotes the excited dimer, which has enough energy to spontaneously dissociate into the two monomers, M is a carrier gas molecule (N_2 or CH_4), and k_1-k_4 are the reaction rate constants. In the equilibrium state, EtOD dimers should be produced through the reaction sequences in Eqs. (36) and (37). According to our hypothesis, the dimer may also be produced in the EtOD/D_2O droplets as

$$\mathrm{A}+\text{droplet}\xrightarrow{k_5}\left(\frac{F_{\text{dimer}}}{2}\right)\mathrm{A}_2+(1-F_{\text{dimer}})\mathrm{A}+\text{droplet}, \tag{38}$$

where F_{dimer} denotes the dimerization efficiency, which is less than or equal to unity. In writing Eq. (38), the growth of the droplet by attachment of the monomer is neglected for simplicity, because it was estimated from the depletion rate of the EtOD monomers and the collision rate between the EtOD monomers and the droplets that the net droplet growth rate is only about 10% of the monomer/droplet collision rate.

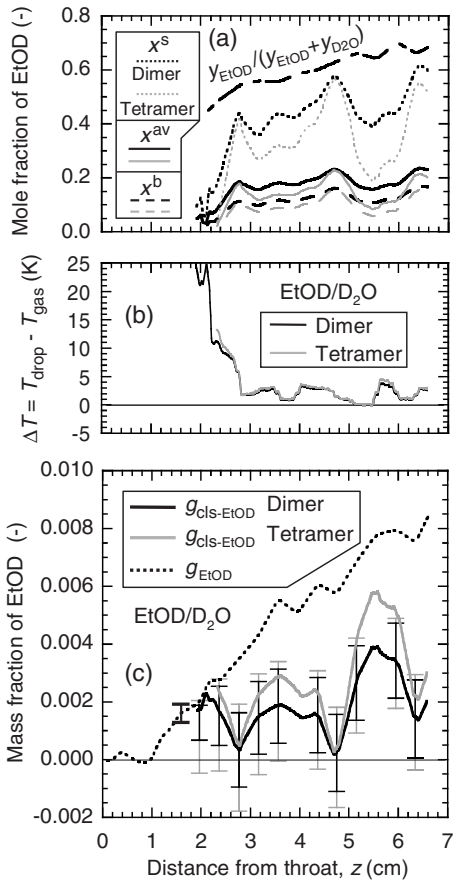

FIG. 9. Results of the determination of mass fraction of EtOD cluster, $g_{cls\text{-EtOD}}$, in the EtOD/D_2O condensing flow for the two cases, where a suitable amount of EtOD dimer (or tetramer) is assumed to be formed so that $\Delta h_{\text{exp}}=\Delta h_{\text{theor}}$ is satisfied. (a) Mole fractions of EtOD in the EtOD/D_2O droplet, average mole fraction, x^{av}, bulk mole fraction, x^b, and surface mole fraction, x^s, these were calculated in the determination process of $g_{cls\text{-EtOD}}$. Mole fraction ratio in vapor phase, $y_{\text{EtOD}}/(y_{\text{EtOD}}+y_{\text{D}_2\text{O}})$, is also shown. (b) Difference of the temperatures between the EtOD/D_2O droplet and gas, ΔT. ΔT was calculated in the determination process of $g_{cls\text{-EtOD}}$. The same $\langle r\rangle$ as that in Fig. 6(b) was used for determining $g_{cls\text{-EtOD}}$ and the extrapolation of $\langle r\rangle$ was not necessary because $g_{cls\text{-EtOD}}$ was determined within the z range, where the measured $\langle r\rangle$ is available. (c) $g_{\text{cls-EtOD}}$ for the two cases, where EtOD dimer (or tetramer) is assumed to be formed. Mass fraction of condensed EtOD determined by LAM, $g_{\text{EtOD}}(=g_{cls\text{-EtOD}}+g_{\text{drop-EtOD}})$ is also shown. The definition of the error bars for $g_{cls\text{-EtOD}}$ of dimer is the same as those in Fig. 6(c).

The dimer formed in Eq. (38) dissociates by the same reactions as those in the vapor phase, that is, by the reverse reactions in Eqs. (36) and (37).

We next compare the production rates of A_2 in the vapor phase [Eq. (37)], P_{2_Vapor}, and in the droplets [Eq. (38)], P_{2_Drop}, at $z=4.0$ cm as an example. P_{2_Vapor} is expressed by

$$P_{2\_Vapor} = k_3[M][A_2^*] = k_3[M](k_1/k_2)[A][A], \quad (39)$$

where quasiequilibrium state between A and A_2^* was assumed. P_{2_Drop} is

$$P_{2\_Drop} = k_5(F_{dimer}/2)[Droplet][A]. \quad (40)$$

In order to determine the P_{2_Vapor} and P_{2_Drop}, we need the collision rate between the molecules and/or particles (clusters and droplets). The collision rate was estimated by using a well known equation,[23] derived for the collision between the rigid spheres with diameters d_A and d_B where the Lennard-Jones diameters[24] were used for the collision diameters, i.e., $d_{EtOD} \approx d_{EtOH} = 4.37$ Å, $d_{D_2O} \approx d_{H_2O} = 2.89$ Å, $d_{N_2} = 3.67$ Å, and $d_{CH_4} = 3.73$ Å. The diameter of the EtOD dimer was estimated as $d_{EtOD(2)} = 2^{1/3} d_{EtOD}$, and that of the droplet was determined by SAXS as shown in Fig. 6(b).

The collision rate between a EtOD monomer and other EtOD monomers was determined to be 5.2×10^6 s^{-1}, and, therefore, $k_1[A]$ was estimated as half of that value, 2.6×10^6 s^{-1}, since the collision of the nth A with the mth A is identical to that of the mth A with the nth A. The dissociation rate of A_2^*, k_2, should have a value similar to the intermolecular vibrational frequency of the dimer. According to the *ab initio* harmonic analysis by Senent *et al.*,[25] the harmonic fundamental of the hydrogen bond stretching in the EtOH dimer is located between 155.3 and 189.4 cm^{-1}, which correspond to the frequencies of 4.66×10^{12} and 5.68×10^{12} s^{-1}, respectively. Hence we expect k_2 is around 5×10^{12} s^{-1}. Using these values we estimate $[A_2^*]/[A] = (k_1/k_2)[A]$ is about $5 \times 10^{-7} \{\approx 2.6 \times 10^6/(5 \times 10^{12})\}$. To determine the value of $k_3[M]$, the collision rate between an EtOD dimer and a carrier gas molecule should be multiplied by a collision efficiency factor, $F_{collision}$, which is less than or equal to unity. Then, $k_3[M]$ is determined to be 8.9×10^8 $F_{collision}$ s^{-1}. As a result, $P_{2\_Vapor}/[A]$ is estimated to be 4×10^2 $F_{collision}$ s^{-1} $(\approx 5 \times 10^{-7} \times 8.9 \times 10^8$ $F_{collision})$.

We estimate the collision rate between a EtOD monomer and the droplets, $k_5[droplet]$, to be 6.6×10^4 s^{-1}. This yields $P_{2\_Drop}/[A] (= k_5 F_{dimer}[droplet]/2)$ equal to 3.3×10^4 F_{dimer} s^{-1}, and the ratio, P_{2_Drop}/P_{2_Vapor}, is determined to be $80 \times (F_{dimer}/F_{collision})$.

The mass fraction of EtOD dimer in the equilibrium state under the conditions at $z=4.0$ cm was determined to be 9×10^{-6}. Multiplying this value by $80 \times (F_{dimer}/F_{collision})$ gives $7 \times 10^{-4} \times (F_{dimer}/F_{collision})$, which agrees with the mass fraction of EtOD dimer at this position estimated from the heat balance, 1.5×10^{-3} [see solid line in Fig. 9(c)] if $(F_{dimer}/F_{collision}) \approx 2$. $F_{collision}$ is generally in the range 0.05–1.0,[22] and then F_{dimer} should range from 0.1 to 1.0. This range of F_{dimer} does not seem to be unrealistic and we can conclude the mechanism of the formation of EtOD clusters expressed by Eq. (35) is possible at least for the dimer formation. Finally, we note that a more detailed mechanistic investigation of the formation of EtOD dimers near droplet surfaces and determining the factor F_{dimer} are beyond the scope of this paper.

The value of $g_{cls\text{-}EtOD}$ at $z \leq 1.6$ cm is not so high compared to those downstream of the onset as shown in Fig. 9(c), even though there should be many $EtOD/D_2O$ clusters that are smaller than the critical cluster. This is consistent with the expectation, noted above, that larger clusters work better as heat absorbers to help EtOD clusters form.

To qualitatively confirm the thermodynamic analysis, we performed preliminary FTIR absorption spectroscopy (1 cm^{-1} resolution) measurements for an $EtOH/H_2O$ condensing flow and a pure EtOH flow in the nozzle under conditions similar to those used in this study. The stagnation pressure and temperature were $p_0 = 30.2$ kPa and $T_0 = 308.2$ K, respectively. The initial mole fractions of EtOH and H_2O in the $EtOH/H_2O$ flow were $(y_{EtOH})_0 = 0.0099$ and $(y_{H2O})_0 = 0.0192$, respectively, so that the pressure and temperature profiles were almost the same as in the $EtOD/D_2O$ flow. In the pure EtOH flow, $(y_{EtOH})_0$ was also 0.0099.

FTIR spectra were measured at $z=2.2$ cm in the $EtOH/H_2O$ flow and at $z=1.0$ cm in the pure EtOH flow. At these positions the gas temperature was 239 ± 1 K and corresponds to the temperature found at $z=2.3$ cm in the $EtOD/D_2O$ flow. The molar densities of the EtOH or EtOD in the EtOH, $EtOH/H_2O$, and $EtOD/D_2O$ experiments were 6.1×10^{-2}, 5.5×10^{-2}, and 5.4×10^{-2} mol/m^3, respectively. That is, the FTIR spectrum in the $EtOH/H_2O$ flow was measured under the similar conditions as those at $z=2.3$ cm in the $EtOD/D_2O$ flow, where the mass fraction of the EtOD dimer is estimated to be about 0.002 as shown in Fig. 9(c) and this mass fraction corresponds to 12% of the total amount of EtOD molecules. On the other hand, in the EtOH flow, the FTIR spectrum was measured at the same temperature as in the cases of $EtOH/H_2O$ and $EtOD/D_2O$, but at about 10% higher number density of ethanol molecules.

In the FTIR spectra, we observed an absorption peak around 1030 cm^{-1} in the $EtOH/H_2O$ flow that was not present in the pure EtOH flow even though the number density of EtOH molecules is higher in the latter case than the former. This wave number is very close to the band position of the dissociation spectrum of the gas-phase EtOH dimer, 1031.4 cm^{-1} (Fig. 5 and Table 2 in Ref. 26), and similar as that of the absorption spectrum of the EtOH dimer in an argon matrix at a temperature of 7 K, 1027.4 cm^{-1} (Fig. 4 and the second column of Table 4 in Ref. 27). The band is assigned to the asymmetric CCO stretching mode coupled with the CH_3 rocking vibration of the proton-acceptor monomer with the trans structure in the EtOH dimer.[27] We observed other peaks at wavenumbers from 1040 to 1100 cm^{-1}. However, the assignment of those peaks is not straightforward, because, in this region, the spectra of the dimer measured by the above two methods show different features and the spectra of the liquid,[28] trimer,[26] and maybe larger clusters overlap, and, therefore, the assignment of the peaks in this wavenumber range is a future task. Although not yet quantitative, our preliminary observations support the hypothesis that the D_2O molecules facilitate the formation of the small EtOD-dominant clusters.

Based on our thermodynamic analysis, we hypothesize that small clusters of pure EtOD are formed in the $EtOD/D_2O$ particle (droplet or cluster) and evaporate from it. To confirm this hypothesis, additional analysis is necessary. We should explain quantitatively why at least about 10% of EtOD molecules form clusters, before and after the onset of condensation, despite changing conditions in the gas phase. We are also interested in how the clustering of EtOD affects the nucleation rate of the $EtOD/D_2O$ mixture. Those quantitative analyses are future tasks, as are more extensive experiments to quantify the size, composition, and concentration of the clusters.

V. SUMMARY AND CONCLUSION

We determined the latent heat released in the condensing flow of $EtOD/D_2O$, Δh_{exp}, using the measurements of pressure, temperature, mole fractions of EtOD monomer, and D_2O monomer, presented in our previous study,[4] by integrating the supersonic flow equations. By considering the depletion of the monomer from the gas phase, the deviation of the pressure from the isentropic value, and Δh_{exp}, we found that, upstream of the onset point of condensation, about 10% of EtOD molecules formed EtOD-dominant clusters, and we estimated that the size of these clusters was in the range of dimer to tetramer. Furthermore, the experimental results suggested that D_2O molecules facilitate the formation of the EtOD-dominant clusters. A comparison between Δh_{exp} and the heat of dissociation of the $EtOD/D_2O$ droplet estimated from the thermodynamic properties of $EtOD/D_2O$ mixture, Δh_{theor}, suggests that even downstream of the onset of condensation, the formation of a detectable amount of clusters occurs.

By considering the temperature and monomer concentrations in the nozzle, the concentrations of those clusters in the nozzle were found to be much higher than those expected in the equilibrium state, both upstream and downstream of the onset point of condensation. In order to explain these observations, a possible mechanism for the clustering was proposed, that is, the pure EtOD cluster is formed in the $EtOD/D_2O$ particle (droplet or cluster), and evaporates from it, with the particle acting as a catalyst. This mechanism is consistent with the mass spectroscopic measurements of Nishi *et al.*[8] and Wakisaka and Ohki.[9] The mass fraction of pure EtOD clusters was determined so that Δh_{exp} agreed with Δh_{theor}, and it was determined that on average at least $\sim 10\%$ of EtOD molecules form clusters downstream of the onset point of condensation.

ACKNOWLEDGMENTS

This work was supported by the National Science Foundation under Grant No. CHE-0410045 and by the Donors of the Petroleum Research Fund administered by the American Chemical Society. We deeply thank Professor S. B. Kiselev for providing the FORTRAN program developed by him for estimation of thermodynamic properties of D_2O in supercooled state.

APPENDIX A: BOUNDARY LAYER

To determine the temperature profile within the boundary layer, we need to decide whether the boundary layers are laminar or turbulent and confirm that boundary layer separation does not occur. As discussed in our earlier publication,[3] under our experimental conditions, the boundary layer in the nozzle is expected to be laminar except in the region of increasing pressure. Under an adverse pressure gradient, the boundary layer either becomes turbulent or separates, regardless of the value of the Reynolds number Re_z.[11(b),29] To determine whether boundary layer separation is possible, we examined the criterion developed by Stratford[30] for flow over a flat plate. The separation position (distance from the leading edge of the flat plate), z_s, is predicted by Eq. (A1).[30]

$$C_{\text{pr}}\left(z_s\frac{dC_{\text{pr}}}{dz}\right)^{1/2} = \begin{cases} 0.39(10^{-6}\,\text{Re}_z)^{1/10} & \text{when} \quad d^2p/dz^2 \geq 0 \\ 0.35(10^{-6}\,\text{Re}_z)^{1/10} & \text{when} \quad d^2p/dz^2 < 0 \end{cases} . \tag{A1}$$

Here C_{pr} and Re_z are the pressure coefficient and Reynolds number, respectively, defined by

$$C_{\text{pr}} \equiv (p - p_{\text{pin}})/(\rho u_{\text{pin}}^2/2), \qquad \text{Re}_z \equiv uz/\nu, \tag{A2}$$

where the subscript pin denotes the value at the position where the pressure starts to increase, and ν is the kinematic viscosity of the gas. We evaluated both sides of Eq. (A1) in the region where $dp/dz > 0$ assuming that the origin, $z=0$, is at the throat of the nozzle, and found that the left hand side is only $\sim 0.1\%$ of the right hand side. Hence, boundary layer separation should not occur although the flow in the boundary layer will become turbulent. Thus, to calculate T from $\langle T \rangle = T_{\text{LAM}}$, we assumed flow in the boundary layer was laminar when $dp/dz \leq 0$ and turbulent when $dp/dz > 0$. To avoid any discontinuity in T when dp/dz changes sign, near a transition point z_t we calculated T for both the laminar and turbulent boundary layer cases, T_{laminar} and $T_{\text{turbulent}}$, and averaged them in the region from z_t to $z_t + 0.1$ cm using $T = T_{\text{laminar}}(z_t + 0.1 - z)/0.1 + T_{\text{turbulent}}(z - z_t)/0.1$ when the sign of dp/dz changes from minus to plus, or using $T = T_{\text{turbulent}}(z_t + 0.1 - z)/0.1 + T_{\text{laminar}}(z - z_t)/0.1$ when the sign changes from plus to minus.

APPENDIX B: THE HEAT OF DISSOCIATION OF THE DROPLETS

The heat of dissociation of the droplets, $\Delta H_{\text{dis}}^{\text{drop}}$, consists of the change in the internal energy, ΔU, and the change in $p^v V$, $p^v \Delta V$, of the system (vapor+droplets), where p^v denotes the pressure in vapor phase, and V is the volume of the system. Initially, the system consists of droplets and vapor with an initial energy equal to $U^v + U^l + U^s$, where U^v and U^l are the internal energies in the vapor and liquid phases, respectively, and U^s denotes the surface energy. The final state consists only of vapor at an energy U_{final}^v. The enthalpy change to dissociate the droplets is then given by

$$\Delta H_{\mathrm{dis}}^{\mathrm{drop}} = \Delta U + p^v \Delta V = U_{\mathrm{final}}^v - (U^v + U^l + U^s) + p^v \Delta V. \tag{B1}$$

The internal energies U_{final}^v, U^v, U^l, and U^s are expressed by Eqs. (B2)–(B5), respectively.[31]

$$U_{\mathrm{final}}^v = \sum_i n_i^{\mathrm{tot}} u_i^v, \tag{B2}$$

$$U^v = \sum_i n_i^v u_i^v, \tag{B3}$$

$$U^l = \sum_i n_i^l u_i^l, \tag{B4}$$

$$U^s = \sum_i n_i^s \mu_i + TS^s + \sigma\Omega, \tag{B5}$$

where n_i^v and n_i^l are the numbers of moles of species i in the initial bulk vapor and liquid phases, respectively, and n_i^s is the surface excess number of moles of species i, such that $n_i^{\mathrm{tot}} = n_i^v + n_i^l + n_i^s$. The partial molar internal energy of species i in the liquid and vapor phases are denoted by u_i^l and u_i^v, respectively, and the chemical potential of species i, μ_i, is assumed to be the same for the liquid phase and the surface. In Eq. (B5), S^s is the surface entropy, σ and Ω denote the surface tension and surface area, respectively.

According to the generalized Gibbs adsorption equation [Eq. (11.8) in Ref. 31], the surface entropy S^s is given by

$$\begin{aligned} S^s &= -\Omega\left(\frac{\partial\sigma}{\partial T}\right)_{r,x_i^l} - \sum_i n_i^s \left(\frac{\partial \mu_i}{\partial T}\right)_{r,x_i^l} \\ &= -\Omega\left(\frac{\partial\sigma}{\partial T}\right)_{r,x_i^l} - \sum_i n_i^s \left\{ -s_i^l + v_i^l \left(\frac{\partial p^l}{\partial T}\right)_{r,x_i^l} \right\}, \end{aligned} \tag{B6}$$

where r is the radius of the droplet and x_i^l denotes the mole fraction of species i in the liquid phase. The variables in the liquid phase, s_i^l, v_i^l, and p^l denote the partial molar entropy of species i, partial molar volume of species i and the pressure, respectively. Substituting Eq. (B6) into Eq. (B5) gives

$$\begin{aligned} U^s &= \sum_i n_i^s \left\{ u_i^l + v_i^l p^l + v_i^l T \left(\frac{\partial p^l}{\partial T}\right)_{r,x_i^l} \right\} + \Omega\left\{ \sigma - T\left(\frac{\partial\sigma}{\partial T}\right)_{r,x_i^l} \right\} \\ &= \sum_i n_i^s u_i^l + \Omega\left\{ \sigma - T\left(\frac{\partial\sigma}{\partial T}\right)_{r,x_i^l} \right\}, \end{aligned} \tag{B7}$$

where the final equation was obtained by adopting the Koenig–Buff dividing surface[32] so that $\Sigma_i n_i^s v_i^l = 0$ is satisfied. As a result, the internal energy of the droplets, $U_{\mathrm{drop}} (= U_l + U_s)$, can be rewritten as

$$\begin{aligned} U_{\mathrm{drop}} &= \sum_i n_i u_i^l + U_{\mathrm{excess}}, \\ U_{\mathrm{excess}} &\equiv \Omega\left\{ \sigma - T\left(\frac{\partial\sigma}{\partial T}\right)_{r,x_i^l} \right\}, \end{aligned} \tag{B8}$$

where n_i is the number of moles of species i in the droplets $(= n_i^l + n_i^s)$. From Eqs. (B1) and (B8), we have

$$\begin{aligned} \Delta H_{\mathrm{dis}}^{\mathrm{drop}} &= \left(U_{\mathrm{final}}^v - U^v - \sum_i n_i u_i^l + p^v \Delta V \right) - U_{\mathrm{excess}} \\ &= \sum_i n_i \Delta h_{\mathrm{vap}\text{-}i}^{\mathrm{bulk}} - U_{\mathrm{excess}}, \end{aligned} \tag{B9}$$

where $\Delta h_{\mathrm{vap}\text{-}i}^{\mathrm{bulk}}$ denotes the partial molar heat of vaporization of species i of the bulk liquid at the composition x_i^l and the pressure p^v. Here, ΔV was assumed to be the same for the vaporization of the bulk liquid and the dissociation of the droplet, that is, the volume of the condensate was assumed to be the same for the bulk liquid with a planar surface and the droplet. Furthermore, the small pressure dependence of u_i^l was neglected.

Because the surface composition and the bulk composition (i.e., liquid phase composition x_i^l) of an ethanol/water droplet will generally differ, we use the explicit cluster model by Laaksonen and Kulmala[14] to determine $\Delta H_{\mathrm{dis}}^{\mathrm{drop}}$ using Eq. (B9). In the cluster model, the bulk mole fraction of ethanol, x^b, and the surface mole fraction x^s of the droplets are derived from the averaged mole fraction x^{av} and the droplet radius r. The surface tension is then given by $\sigma(T, x^b)$ instead of $\sigma(T, x^{\mathrm{av}})$, where the function $\sigma(T,x)$ is the same as that for the bulk liquid. It is noted that the x^b in the explicit cluster model corresponds to the x_{ethanol}^l in Eqs. (B6)–(B9). The summation $\Sigma_i n_i \Delta h_{\mathrm{vap}\text{-}i}^{\mathrm{bulk}}$ for EtOD/D_2O mixture is given by

$$\sum_i n_i \Delta h_{\mathrm{vap}\text{-}i}^{\mathrm{bulk}} = n_{\mathrm{EtOD}} \Delta h_{\mathrm{vap\text{-}EtOD}}^{\mathrm{bulk}}(T, x^b) + n_{\mathrm{D_2O}} \Delta h_{\mathrm{vap\text{-}D_2O}}^{\mathrm{bulk}}(T, x^b), \tag{B10}$$

where $\Delta h_{\mathrm{vap}\text{-}i}^{\mathrm{bulk}}$ denotes the partial molar heat of vaporization of species i in the EtOD/D_2O bulk liquid. $\Delta h_{\mathrm{vap}\text{-}i}^{\mathrm{bulk}}$ is given by

$$\begin{aligned} &\Delta h_{\mathrm{vap}\text{-}i}^{\mathrm{bulk}}(T,x) = \frac{\partial}{\partial n_i'} \{ (n'_{\mathrm{EtOD}} + n'_{\mathrm{D_2O}}) \Delta h_{\mathrm{vap}}^{\mathrm{bulk}}(T,x) \}, \\ &i = \mathrm{EtOD}, \mathrm{D_2O}, \\ &x = n'_{\mathrm{EtOD}} / (n'_{\mathrm{EtOD}} + n'_{\mathrm{D_2O}}), \end{aligned} \tag{B11}$$

$$\begin{aligned} \Delta h_{\mathrm{vap}}^{\mathrm{bulk}}(T,x) = {} & x \Delta h_{\mathrm{vap\text{-}EtOD}}^{\mathrm{bulk/pure}}(T) + (1-x) \Delta h_{\mathrm{vap\text{-}D2O}}^{\mathrm{bulk/pure}}(T) \\ & - \Delta h_{\mathrm{mix}}(T,x), \end{aligned}$$

where $\Delta h_{\mathrm{vap}}^{\mathrm{bulk}}(T,x)$ is the molar heat of vaporization of bulk EtOD/D_2O liquid. $\Delta h_{\mathrm{vap}\text{-}i}^{\mathrm{bulk/pure}}$ is the molar heat of vaporization of pure liquid of species i, and Δh_{mix} denotes the molar mixing enthalpy.

Finally, dividing Eq. (B9) by $(n_{\mathrm{EtOD}} + n_{\mathrm{D2O}})$ gives the molar heat of dissociation of the droplet as

$$\begin{aligned} \Delta h_{\mathrm{dis}}^{\mathrm{drop}} = {} & x^{\mathrm{av}} \Delta h_{\mathrm{vap\text{-}EtOD}}^{\mathrm{bulk}}(T,x^b) + (1-x^{\mathrm{av}}) \Delta h_{\mathrm{vap\text{-}D_2O}}^{\mathrm{bulk}}(T,x^b) \\ & - \{ \sigma(T,x^b) - T(\partial\sigma/\partial T) \} a, \end{aligned} \tag{B12}$$

where a is the surface area per unit mole of condensate. Assuming the droplets are spherical, a is calculated as

$$a = \frac{\langle 4\pi r^2 \rangle}{\langle (4/3)\pi r^3 / v_m \rangle} = \frac{3v_m}{\langle r \rangle} \frac{Z+1}{Z+3}, \tag{B13}$$

where the brackets $\langle \cdots \rangle$ denote the number average and v_m is the molar volume of condensate in the droplet. In contrast with σ and $\Delta h_{\text{vap-}i}^{\text{bulk}}$, v_m was assumed to equal that of the bulk liquid at x^{av}. The number average radius of the droplet, $\langle r \rangle$, was determined by XSM assuming that the aerosol particle size distribution follows the Schultz distribution [Eq. (1)]. The average value of the parameter Z was determined to be 18.1 and this value was used for Z at all positions in the nozzle. In Eq. (B13), the relations, $\langle r^2 \rangle = \langle r \rangle^2 (Z+2)/(Z+1)$ and $\langle r^3 \rangle = \langle r \rangle^3 (Z+2)(Z+3)/(Z+1)^2$, were used. We note that, for simplicity, we neglected the effect of the distribution of r on x^b and used $r = \langle r \rangle$ to estimate this composition.

In the case where the temperature of the droplet, T_{drop}, may be different from that of the gas, T_{gas}, the molar heat of dissociation of the droplet in the nozzle, Δh_{theor}, is determined by Eq. (B14).

$$\Delta h_{\text{theor}} = \Delta h_{\text{dis}}^{\text{drop}}(T_{\text{drop}}) - \int_{T_{\text{gas}}}^{T_{\text{drop}}} \{x^{\text{av}} C_{p\text{-EtOD}(v)}^0 + (1 - x^{\text{av}}) C_{p\text{-D}_2\text{O}(v)}^0\} dT. \tag{B14}$$

The droplet temperature T_{drop} can be estimated from an energy balance on droplets of size $\langle r \rangle$. Under the conditions of this study, the Knudsen number, $\text{Kn} \equiv \lambda / r$, where λ is the mean free path of the gas molecules, ranges from 70 to 470. Thus, the gas-droplet mixture is in the free molecule regime,[33] and the heat flux from a droplet due to the collision with a noncondensing species α, $J_{q,\alpha}$ can be estimated by[34]

$$J_{q,\alpha} = \pi \langle r^2 \rangle \left(\frac{8RT_{\text{gas}}}{\pi \mu_\alpha} \right)^{1/2} \frac{p_\alpha}{RT_{\text{gas}}} \left(C_{v-\alpha(v)} + \frac{R}{2} \right) (T_{\text{drop}} - T_{\text{gas}}), \tag{B15}$$

where μ_α and $C_{v-\alpha(v)}$ are the molecular weight and the constant volume molar heat capacity of species α in the vapor phase, respectively, and R is the gas constant. p_α is the partial pressure of species α. In our experiments α corresponds to N_2 and CH_4 and we ignore any potential contribution of the condensing species, D_2O and EtOD, to heat transfer, because the initial mole fractions of EtOD and D_2O are only 0.0097 and 0.0146, respectively. In the absence of clustering, under the quasisteady state assumption, the heat transfer from the droplets to the surrounding gas must balance the measured heat release to the flow, dq, and the dq' due to the temperature change of the gas, i.e.,

$$N_c \sum_\alpha J_{q,\alpha} = d(q + q')/dt = dq/dt - (dT_{\text{gas}}/dt) \sum_i g_i c_{p-i(v)}^0, \tag{B16}$$

where N_c is the number of droplets per unit mass of the gas mixture, and it is obtained by

$$N_c = \frac{V_c}{(4/3)\pi \langle r^3 \rangle}, \tag{B17}$$

where V_c is the volume of the droplets per unit mass of gas mixture and it is given by Eq. (24). When we consider the effect of clustering, V_c is determined using $g_{\text{drop-}i}$ instead of g_i as described in Sec. III D. However, in Eq. (B16), not q_{drop} and $g_{\text{drop-}i}$ but q and g_i are used to estimate the heat transfer from the droplets to the surrounding gas, because we hypothesize the most clusters are produced in the droplets.

It is noted that the effect of the clustering in vapor phase on $\Delta h_{\text{vap-}i}^{\text{bulk/pure}}$ is negligible under the conditions in this study as explained below. Generally, the heat of vaporization of the bulk liquid is measured under the equilibrium condition, and then the effect of the clustering in vapor phase on it becomes significant near the normal boiling temperature (T_b), because the equilibrium vapor pressure at that temperature is very high (atmospheric pressure) and many clusters are produced. However, the difference between the enthalpies of the ideal gas and saturated vapor is completely negligible at the temperature below ($T_b - 100$ K).[35] The values of T_{drop} estimated in this study satisfy this condition both for EtOD ($T_b = 352$ K) and D_2O ($T_b = 375$ K) except for the fluctuations just downstream of the onset point of condensation. Therefore, we can expect that the Δh_{theor} in Eq. (B14) does not include the effect of the clustering even if the value of $\Delta h_{\text{vap-}i}^{\text{bulk/pure}}$ for the saturated vapor is used.

APPENDIX C: THERMODYNAMIC PROPERTIES OF THE PURE COMPONENTS AND EtOD/D_2O MIXTURES

This appendix summarizes the relevant thermodynamic properties of the pure species, EtOD, D_2O, CH_4, and N_2, as well as those of the EtOD/D_2O mixtures. For the mixtures, the molar volume, surface tension, and mixing enthalpy are estimates based on the properties of EtOH/D_2O or EtOH/H_2O mixtures. Since the contributions to Δh_{theor} that depend on mixture properties are rather small, our approximations should not significantly affect the conclusions drawn in this work.

1. Heat of vaporization of pure EtOD, $\Delta h_{\text{vap-EtOD}}^{\text{bulk/pure}}$

The vapor pressure of EtOD is reported as (Refs. 36 and 37, respectively)

$$\ln(p_{\text{EtOH}}/\text{Torr}) = 64.276 - 7055.31/T - 6.41 \ln T \quad \text{for } 243.15 \le T/\text{K} \le 350,$$

$$\ln(p_{\text{EtOH}}/p_{\text{EtOD}}) = 18343/T^2 - 44.45/T \quad \text{for } 258.2 \le T/\text{K} \le 351.2.$$

Hence, $\Delta h_{\text{vap-EtOD}}^{\text{bulk/pure}}$ can be determined by applying the Clausius–Clapeyron equation as

$$\Delta h_{\text{vap-EtOD}}^{\text{bulk/pure}}(T) = RT^2 \frac{d \ln p_{\text{EtOD}}}{dT} = R(36686T^{-1} + 7010.86 - 6.41T) \quad \text{(J/mol)} \quad \text{for } 258.2 \le T/\text{K} \le 350. \tag{C1}$$

$\Delta h_{\text{vap-EtOD}}^{\text{bulk/pure}}$ at $T<258.2$ K was estimated as follows. Isobaric molar heat capacity of EtOD vapor, $C_{p\text{-EtOD}(v)}^{0}$, and that of EtOD liquid, $C_{p\text{-EtOD}(l)}$, are expressed by Eqs. (C2) and (C3), respectively.

$$C_{p\text{-EtOD}(v)}^{0} = 30.941 + 0.10037T + 7.322\times10^{-5}T^{2} \quad \text{(J/mol K)} \quad \text{for} \quad 100 \le T/\text{K} \le 400, \tag{C2}$$

$$C_{p\text{-EtOD}(l)} = 117.64 - 0.36163T + 1.1963\times10^{-3}T^{2} \quad \text{(J/mol K)} \quad \text{for} \quad 160 \le T/\text{K} \le 250, \tag{C3}$$

where Eqs. (C2) and (C3) were obtained by fitting quadratic functions to the calculated values[38] of $C_{p\text{-EtOD}(v)}^{0}$ at $T=100-400$ K in the ideal gas state (i.e., at infinitely low pressure), and to the measured values[39] of $C_{p\text{-EtOD}(l)}$ at $T=160-250$ K, respectively. The temperature derivative of $\Delta h_{\text{vap-EtOD}}^{\text{bulk/pure}}$ can be determined from these two heat capacities by using Kirchhoff's equation[12] as

$$\frac{d\{\Delta h_{\text{vap-EtOD}}^{\text{bulk/pure}}(T)\}}{dT} = C_{p\text{-EtOD}(v)}^{0} - C_{p\text{-EtOD}(l)} = -86.70 + 0.4620T - 1.1231\times10^{-3}T^{2} \quad \text{(J/mol K)} \quad \text{for} \quad 160 \le T/\text{K} \le 250. \tag{C4}$$

As indicated by Eqs. (C1) and (C4), data at $T=250-258.2$ K are missing. Hence, $\Delta h_{\text{vap-EtOD}}^{\text{bulk/pure}}$ at $T=250-260$ K was interpolated by a quadratic function, $f_{\text{inter}}(T)$, which satisfy the following three equations: $f_{\text{inter}} = \Delta h_{\text{vap-EtOD}}^{\text{bulk/pure}}$ at 260 K, and $df_{\text{inter}}/dT = d\Delta h_{\text{vap-EtOD}}^{\text{bulk/pure}}/dT$ at $T=250$ and 260 K. The obtained interpolating function is expressed by

$$f_{\text{inter}}(T) = 5.45\times10^{3} + 366.7T - 8.164\times10^{-1}T^{2} \quad \text{(J/mol)} \quad \text{for} \quad 250 \le T/\text{K} \le 260. \tag{C5}$$

2. Heat of vaporization of pure D_2O, $\Delta h_{\text{vap-D}_2\text{O}}^{\text{bulk/pure}}$

The vapor pressure of D_2O is reported[40] as

$$\ln(p_{\text{D}_2\text{O}}/p_c) = (T_c/T)(A_1\tau + A_2\tau^{1.9} + A_3\tau^{2} + A_4\tau^{5.5} + A_5\tau^{10}), \quad \tau \equiv 1 - T/T_c \quad \text{for} \quad 275 \le T/\text{K} \le 823, \tag{C6}$$

where $A_1=-7.815\,83$, $A_2=17.6012$, $A_3=-18.1747$, $A_4=-3.924\,88$, $A_5=4.191\,74$, $p_c=21.66$ MPa, and $T_c=643.89$ K. We found that this equation reproduced the experimental value[41] of $p_{\text{D}_2\text{O}}$ at $T=258-276$ K with a root-mean-square error of 0.88%. Hence, Eq. (C6) can be applied over the temperature range of 258–823 K. $\Delta h_{\text{vap-D}_2\text{O}}^{\text{bulk/pure}}$ can be determined by applying the Clausius–Clapeyron equation similarly as Eq. (C1). $\Delta h_{\text{vap-D}_2\text{O}}^{\text{bulk/pure}}$ at $T<258$ K was estimated from the isobaric molar heat capacities of D_2O vapor and liquid, $C_{p\text{-D}_2\text{O}(v)}^{0}$ and $C_{p\text{-D}_2\text{O}(l)}$, similarly as Eq. (C4). A cubic function was fitted to the calculated values[42] of $C_{p\text{-D}_2\text{O}(v)}^{0}$ at $T=160-340$ K in the ideal gas state, and Eq. (C7) was obtained.

$$C_{p\text{-D}_2\text{O}(v)}^{0} = R(4.171 - 2.239\times10^{-3}T + 8.610\times10^{-6}T^{2} - 5.630\times10^{-9}T^{3}) \quad \text{(J/mol K)} \quad \text{for} \quad 160 \le T/\text{K} \le 340. \tag{C7}$$

$C_{p\text{-D}_2\text{O}(l)}$ was calculated using a FORTRAN program, which was developed by Kiselev and Ely[43] for estimation of the thermodynamic properties of D_2O in the supercooled state based on a parametric crossover model, CREOS-02. At pressures less than 100 kPa, this model can be applied at $T \gtrsim 220$ K. The calculated result is shown in Fig. 2 of Ref. 43. $(C_{p\text{-D}_2\text{O}(v)}^{0} - C_{p\text{-D}_2\text{O}(l)})$ was integrated from $T=270$ to 220 K and a quartic function was fitted to the result as expressed by Eq. (C8).

$$\Delta h_{\text{vap-D}_2\text{O}}^{\text{bulk/pure}} = 63.54 - 0.8384(T-200) + 1.7988\times10^{-2}(T-200)^{2} - 1.8394\times10^{-4}(T-200)^{3} + 7.085\times10^{-7}(T-200)^{4} \quad \text{(kJ/mol)} \quad \text{for} \quad \sim 220 \le T/\text{K} \le 270. \tag{C8}$$

3. Isobaric molar heat capacities of EtOH and H_2O liquid, $C_{p\text{-EtOH}(l)}$ and $C_{p\text{-H2O}(l)}$

A quartic function was fitted to the measured value[44] of $C_{p\text{-EtOH}(l)}$ at $T=158.5-350$ K and Eq. (C9) was obtained.

$$C_{p\text{-EtOH}(l)} = -40.86 + 2.158T - 1.3517\times10^{-2}T^{2} + 3.635\times10^{-5}T^{3} - 3.193\times10^{-8}T^{4} \quad \text{(J/mol K)} \quad \text{for} \quad 158.5 \le T/\text{K} \le 350. \tag{C9}$$

$C_{p\text{-H}_2\text{O}(l)}$ at $T=167-231$ K is given[45] by Eq. (C10).

$$C_{p\text{-H}_2\text{O}(l)} = 38\,565.2 - 635.6299T + 0.964\,911T^{2} + 3.646\,245\times10^{-2}T^{3} - 2.189\,861\times10^{-4}T^{4} + 4.197\,441\times10^{-8}T^{5} + 2.456\,321\times10^{-9}T^{6} - 4.839\,049\times10^{-12}T^{7} \quad \text{(J/mol K)} \quad \text{for} \quad 167 \le T/\text{K} \le 231. \tag{C10}$$

$C_{p\text{-H}_2\text{O}(l)}$ at $T \gtrsim 231$ K was estimated from $\Delta h_{\text{vap-H}_2\text{O}}^{\text{bulk/pure}}$ and $C_{p\text{-H}_2\text{O}(v)}^{0}$ by using Kirchhoff's law similarly as Eq. (C4). $\Delta h_{\text{vap-H}_2\text{O}}^{\text{bulk/pure}}$ and $C_{p\text{-H}_2\text{O}(v)}^{0}$ are given by Eq. (C11) (Ref. 45) and Eq. (C12), respectively.

$$\Delta h_{\text{vap-H}_2\text{O}}^{\text{bulk/pure}} = 56\,579 - 42.212T + \exp\{0.1149(281.6-T)\} \quad \text{(J/mol)} \quad \text{for} \quad 231 \le T/\text{K} \le 273.16, \tag{C11}$$

$$C^0_{p\text{-}H_2O(v)} = R(3.995 + 2.688 \times 10^{-4}T - 2.104 \times 10^{-6}T^2 + 5.658 \times 10^{-9}T^3) \quad \text{(J/mol K)} \quad \text{for} \quad 160 \le T/\text{K} \le 340, \tag{C12}$$

where Eq. (C12) was obtained by fitting a cubic function to the calculated values[42] of $C^0_{p\text{-}H_2O(v)}$at $T=160-340$ K. The obtained $C_{p\text{-}H_2O(l)}$ is expressed by Eq. (C13),

$$C_{p\text{-}H_2O(l)} = 75.43 + 2.235 \times 10^{-2}T - 1.749 \times 10^{-5}T^2 + 4.705 \times 10^{-8}T^3 + 0.1149 \times \exp\{0.1149(281.6 - T)\} \quad \text{(J/mol K)} \quad \text{for} \quad 231 \le T/\text{K} \le 285. \tag{C13}$$

It was found that the Eq. (C13) agrees with the experimental result[46] at $T=236-285$ K with a root-mean-square error of 0.2%. Hence Eq. (C13) can be used at $T=231-285$ K.

4. Isobaric molar heat capacities of N_2 and CH_4 vapor, $C_{p\text{-}N_2(v)}$ and $C_{p\text{-}CH_4(v)}$

The temperature and pressure dependencies of the heat capacity of the carrier gas were neglected in this study. The following values were used (Refs. 47 and 48, respectively).

$$C_{p\text{-}N_2(v)} = 29.124 \ \text{J/mol K} \quad \text{at} \quad p_{N_2} = 1 \ \text{atm}$$

and $T = 298.15$ K,

$$C_{p\text{-}CH_4(v)} = 35.7 \ \text{J/mol K} \quad \text{at} \quad p_{CH_4} = 100 \ \text{kPa}$$

and $T = 298.15$ K.

5. Molar volume v_m of EtOD/D_2O

Experimental values of the molar volume of EtOD/D_2O mixtures, $v_{m\text{-}EtOD/D_2O}$ are not available, and are therefore assumed to be the same as $v_{m\text{-}EtOH/D_2O}$. This approximation should be good because, at $T=20$ °C, $v_{m\_EtOD} = 47.07/\rho_{EtOD} = 58.36$ cm^3/mol is very close to $v_{m\text{-}EtOH} = 46.07/\rho_{EtOH} = 58.47$, where $\rho_{EtOD}=0.8050$ g/cm^3 (Ref. 39) and $\rho_{EtOH}=0.7894$ (Ref. 47). $v_{m\text{-}EtOD/D_2O}$ ($T=25$ °C, x_{EtOD}) is estimated as

$$v_{m\text{-}EtOD/D_2O}(T = 25\ ^\circ\text{C}, x_{EtOD}) \approx v_{m\text{-}EtOH/D_2O}(T = 25\ ^\circ\text{C}, \quad x_{EtOH} = x_{EtOD}) = \{46.07x_{EtOD} + 20.03(1 - x_{EtOD})\}/\rho_{EtOH/D_2O}(T = 25\ ^\circ\text{C}, \quad x_{EtOH} = x_{EtOD}). \tag{C14}$$

The density of EtOH/D_2O at $T=25$ °C was measured in Ref. 49 by the density meter (DA-110M, Mettler Toledo) and a quartic function was fitted[49] as

$$\rho_{EtOH/D_2O}(T = 25\ ^\circ\text{C}, x_{EtOH}) = 1.104 - 0.6164x_{EtOH} + 0.3234x^2_{EtOH} + 0.0815x^3_{EtOH} - 0.1055x^4_{EtOH} \quad (\text{g/cm}^3). \tag{C15}$$

The temperature dependence of $v_{m\text{-}EtOD/D_2O}$ was neglected. Sorensen measured the density of EtOH/H_2O solutions ($x_{EtOH} \le 0.2$) at $T=233-323$ K.[50] According to these results, when temperature decreases from 298 K (25 °C) to 233 K, the change in the density from the value at $T=298$ K ranges from −4.2% to +4.3%. At $x_{EtOH} \ge 0.1$, the temperature dependence becomes more significant for larger x_{EtOH}, that is, $\{\rho(233\ \text{K}) - \rho(298\ \text{K})\}/\rho(298\ \text{K})$ increases with the increase in x_{EtOH}. For pure EtOH, $\{\rho(233\ \text{K}) - \rho(298\ \text{K})\}/\rho(298\ \text{K}) = 7.0\%$ and $\{\rho(223\ \text{K}) - \rho(298\ \text{K})\}/\rho(298\ \text{K}) = 8.1\%$.[51] In this study, the temperature of the droplet was estimated to be higher than 225 K. Therefore, we can expect the accuracy of $v_{m\text{-}EtOD/D_2O}$ is better than 5% under typical conditions ($x_{EtOD} < 0.3$) even if the temperature dependence is neglected.

6. Surface tension σ of EtOD/D_2O mixtures

To our knowledge, there are no available data about σ of EtOD/D_2O. Therefore, data for σ of EtOH/H_2O are used instead. The difference between σ for H_2O and D_2O decreases with the decrease in temperature, that is, at $T=323$, 303, and 283 K, $(\sigma_{D_2O} - \sigma_{H_2O})/\sigma_{H_2O} = -0.026$, −0.018, and −0.015, respectively.[52] Therefore, we can expect that the difference between the surface tensions of H_2O and D_2O at $T < 260$ K is less than a few percent. For larger molecules, ethanol, the difference of surface tension between EtOH and EtOD is expected to be less significant. Hence we use the surface tension of EtOH/H_2O to estimate the surface energy of EtOD/D_2O droplet in an approximate manner. The error caused by this approximation is expected to be less than a few percent.

σ is a function of T and x_{EtOH}. The measured values for $263 \le T \le 330$ K and $0 \le x_{EtOH} \le 1$ are available in Ref. 53. A straight line fit was used to express the temperature dependence of σ for each x_{EtOH}. The correlation coefficient was higher than 0.993 and the average was 0.998. The fitted lines were extrapolated to temperatures as low as 225 K, for analysis in this study. This extrapolation is expected to be a good approximation because σ of most liquids decreases with increasing temperature in a nearly linear fashion except when T is too close to the critical temperature.[54] Furthermore, according to this linear dependence of σ on the temperature, the excess internal energy per unit area, $U_{excess}/\Omega = \sigma - T(\partial\sigma/\partial T)$ [see Eq. (B8)], can be approximated by the extrapolated value of σ at $T=0$ K, that is, U_{excess}/Ω is independent of T.[54] The surface tension $\sigma(T, x_{EtOH})$, where $(x_{EtOH})_i < x_{EtOH} < (x_{EtOH})_{i+1}$, is estimated by the linear interpolation between the measurements, $\sigma(T, (x_{EtOH})_i)$ and $\sigma(T, (x_{EtOH})_{i+1})$.

7. Mixing enthalpy Δh_{mix} of EtOD/D_2O mixtures

To our knowledge, the mixing enthalpy of EtOD/D_2O mixture is reported only for the case at $T=298.15$ K,[55] which is compared with the reported value[56] of that of the EtOH/H_2O mixture at the same temperature in Fig. 10. As shown in the figure, Δh_{mix} of EtOD/D_2O gives close agreement with that of EtOH/H_2O in the whole range of the mole fraction of ethanol. Therefore, this agreement is not expected to be an accidental coincidence at this temperature, and,

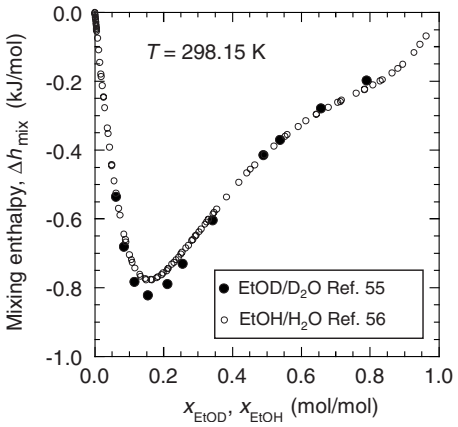

FIG. 10. Mixing enthalpies of the ethanol/water mixtures.

hence, we assumed that Δh_{mix} of $\mathrm{EtOD/D_2O}$ is the same as that of $\mathrm{EtOH/H_2O}$ all over the temperature range in this study, 225–260 K.

Temperature dependence of the Δh_{mix} of $\mathrm{EtOH/H_2O}$ was determined by Eqs. (C16) and (C17) along the method in Ref. 57.

$$\Delta h_{\mathrm{mix}}(T,x_{\mathrm{EtOH}}) = \Delta h_{\mathrm{mix}}(283\ \mathrm{K},x_{\mathrm{EtOH}}) + \int_{283}^{T} \frac{d(\Delta h_{\mathrm{mix}})}{dT} dT, \tag{C16}$$

$$\frac{d(\Delta h_{\mathrm{mix}})}{dT} = C_{p\text{-mix}(l)} - x_{\mathrm{EtOH}} C_{p\text{-EtOH}(l)} - (1 - x_{\mathrm{EtOH}}) C_{p\text{-H}_2\mathrm{O}(l)}, \tag{C17}$$

where $C_{p\text{-mix}(l)}$, $C_{p\text{-EtOH}(l)}$, and $C_{p\text{-H}_2\mathrm{O}(l)}$ are the isobaric molar heat capacity of the $\mathrm{EtOH/H_2O}$ liquid mixture, of the EtOH liquid, and of the $\mathrm{H_2O}$ liquid, respectively. $C_{p\text{-EtOH}(l)}$, and $C_{p\text{-H}_2\mathrm{O}(l)}$ are given above in this appendix. $C_{p\text{-mix}(l)}$ was measured by Westh and Hvidt[57] over a temperature range of 241–293 K and a range of x_{EtOH}, 0.022–1.0 mol/mol. The temperature dependence of $C_{p\text{-mix}(l)}$ at each mole fraction $(x_{\mathrm{EtOH}})_i$ was expressed by a cubic function and this function was extrapolated up to 225 K for analysis in this study. $C_{p\text{-mix}(l)}(T,x_{\mathrm{EtOH}})$, where $(x_{\mathrm{EtOH}})_i < x_{\mathrm{EtOH}} < (x_{\mathrm{EtOH}})_{i+1}$, is estimate by the linear interpolation between $C_{p\text{-mix}(l)}\ (T,(x_{\mathrm{EtOH}})_i)$ and $C_{p\text{-mix}(l)}(T,(x_{\mathrm{EtOH}})_{i+1})$. When $x_{\mathrm{EtOH}} < 0.022$, interpolation can be done between $C_{p\text{-H}_2\mathrm{O}(l)}(T)$ and $C_{p\text{-mix}(l)}(T,0.022)$. $\Delta h_{\mathrm{mix}}(283\ \mathrm{K},x_{\mathrm{EtOH}})$ is expressed by Eq. (C18), the parameters of which were obtained by fitting this function to the experimental data[58] at $x_{\mathrm{EtOH}}=0.05-0.95$.

$$\begin{aligned}\Delta h_{\mathrm{mix}}(283\ \mathrm{K},x_{\mathrm{EtOH}}) &= x_{\mathrm{EtOH}}(1-x_{\mathrm{EtOH}})(-15.254 + 71.009x_{\mathrm{EtOH}} \\ &\quad - 151.750x_{\mathrm{EtOH}}^2 + 152.820x_{\mathrm{EtOH}}^3 \\ &\quad - 59.515x_{\mathrm{EtOH}}^4)\quad (\mathrm{kJ/mol}).\end{aligned} \tag{C18}$$

APPENDIX D: CORRECTION FOR TEMPERATURE DIFFERENCE BETWEEN TDLAS AND SAXS

As described in the previous paper,[4] the inlet temperature of the gas mixture was measured by a platinum resistance thermometer (RTD) in the plenum, which is connected to the inlet of the nozzle. However, the actual inlet temperature T_0, determined by spectroscopy, was between the temperature measured by the RTD, $(T_0)_{\mathrm{RTD}}$, and room temperature T_{room} because of a bypass flow problem in the plenum.

In both the TDLAS (LAM) and SAXS measurements (XSM), $(T_0)_{\mathrm{RTD}}$ was set at 308.2 K. However, in the LAM of the $\mathrm{EtOD/D_2O}$ condensing flow, T_0 was spectroscopically determined to be 303.7 K when T_{room} was 298–299 K. In XSM, T_{room} was ranged from 307 to 309 K, that is, the difference between T_{room} and $(T_0)_{\mathrm{RTD}}$ was within ± 1 K. As shown in the previous paper,[4] the difference between T_0 and $(T_0)_{\mathrm{RTD}}$ was up to 5 K when the difference between T_{room} and $(T_0)_{\mathrm{RTD}}$ was 10 K. Therefore, the difference between T_0 and $(T_0)_{\mathrm{RTD}}$ in the XSM is expected to be within ± 0.5 K $(=\pm 5\ \mathrm{K}/10)$, that is, $T_0=(T_0)_{\mathrm{RTD}} \pm 0.5\ \mathrm{K} = 308.2 \pm 0.5$ K. In this study, we use the radius of the droplet determined by XSM to estimate the surface energy and mixing enthalpy of the droplet. The formation and growth of the droplet should depend on the temperature, and, therefore, the profile of the radius of the droplet in the XSM should be different from that in the LAM. The profile of the radius in the LAM at $T_0=303.7$ K was estimated from the profile determined by XSM at $T_0=308.2$ K as follows.

1. Onset point of condensation

In order to estimate the onset point of condensation in the XSM at $T_0=308.2$ K, onset condition (onset temperature, T_{on}, and onset partial pressure of condensable species, p_{von}) for $\mathrm{EtOD/D_2O}$ at $x_{\mathrm{EtOD}}=0.40$ mol/mol should be given. That is, the Wilson plot, $\ln(p_{\mathrm{von}})$ versus T_{on}, should be given. The intersection of the onset line $(T_{\mathrm{on}},p_{\mathrm{von}})$ and the isentrope $(T_{\mathrm{is}},p_{\mathrm{vis}})$ is the onset point, where p_{vis} is the isentropic partial pressure of the condensable species. According to our previous studies,[6] in this appendix, the onset point of condensation was defined as the position where the temperature exceed the isentropic temperature by 0.5 K.

The onset condition in the LAM was $T_{\mathrm{on}}=230.6$ K and $p_{\mathrm{von}}=0.274$ kPa. These data are shown in Fig. 11 (closed circle) with the Wilson plots under the various conditions. Three fitted linear lines are shown for (1) $\mathrm{D_2O}$ in nozzle A$(d(A/A^*)/dz=0.049\ \mathrm{cm^{-1}})$ at $p_0=59.7$ kPa (open triangle), (2) $\mathrm{D_2O}$ in nozzle H$(d(A/A^*)/dz=0.054\ \mathrm{cm^{-1}})$ at $p_0=30.2$ kPa (closed triangle), and (3) $\mathrm{EtOH/D_2O}$ ($x_{\mathrm{EtOH}}=0.60$) in nozzle A at $p_0=59.7$ kPa, respectively. The difference of the slope of the lines (1) and (2) is only 1.3%, that is, the difference of the slope between the two conditions, (nozzle A, $p_0=59.7$ kPa) and (nozzle H, $p_0=30.2$ kPa) is insignificant, though the intercepts are well different. Similarly, the difference of the slope of lines (1) and (3) is only 5.2% despite the large difference of the composition between $x_{\mathrm{EtOH}}=0$ for line (1) and $x_{\mathrm{EtOH}}=0.6$ for line (3). Therefore, the dependence of the slope on x_{EtOH} is also insignificant. Furthermore, the condensation behavior of $\mathrm{EtOD/D_2O}$ is ex-

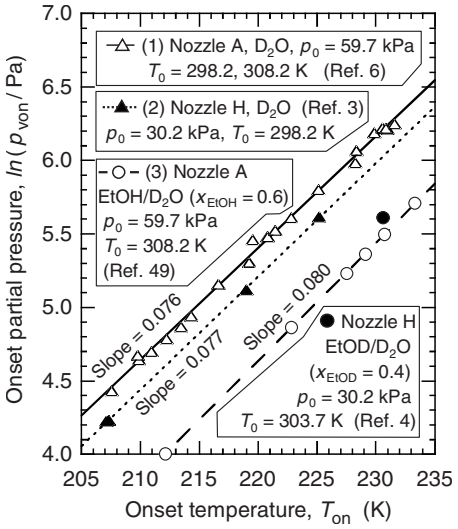

FIG. 11. Wilson plots at different conditions. Nozzle H was used in the present study. The effective shape of the nozzle, $d(A/A^*)/dz$, is 0.049 cm^{-1} for nozzle A at p_0=59.7 kPa (Ref. 6), and 0.054 cm^{-1} for nozzle H at p_0 =30.2 kPa.

pected to be similar to EtOH/D_2O, because the molecular weight of EtOD is only 2% higher than EtOH. Therefore, the slope of the Wilson plot for EtOD/D_2O (x_{EtOD}=0.40) is expected to be close to that of line (1) or (3). We estimated the onset point for two cases, when the slope of the Wilson plot is the same as that of line (1) or (3), and found that the difference of the onset point (distance from throat) was only 0.005 cm. Hence, we can estimate the onset point to a good approximation by assuming that the slope of the Wilson plot is the same as that of the line (3), $d\ln(p_{von}/Pa)/dT_{on}$ =0.080 K^{-1}. As a result, the onset point in the XSM (T_0 =308.2 K) was estimated to be z=1.70 cm, 0.34 cm downstream of the onset point in the LAM (T_0=303.7 K), z =1.36 cm. As shown in Fig. 5, the starting point of the rapid increase in q is z=1.6 cm, which is different from the onset point determined here from the deviation of T from T_{is}, z =1.36 cm. Though the onset point may depend on the criteria, the distance between the onset points at different T_0 is not expected to depend on the criteria so much. Therefore, the difference of the onset point between LAM and XSM, 0.34 cm, which was estimated above, will be used in this appendix for correcting the difference of T_0 between the two measurements without paying attention to the criteria of the onset point.

2. Number density of the droplet

As well known, typically, the nucleation rate exponentially increases with the decrease in temperature and/or the increase in the monomer concentration. However, the number density of the droplet produced in the supersonic Laval nozzle is insensitive to the stagnation conditions, that is, stagnation temperature, T_0, and the initial mole fraction of condensable species, $(y_v)_0$.[6,59,60] For example, in the case of the condensation of D_2O in the nozzle A, the number density of D_2O droplet at z=5.6 cm was in the narrow range, N =4.13×10^{11}–1.02×10^{12} cm^{-3}, even when the stagnation conditions were changed over a wide range of T_0 =298.2–318.2 K and $(y_{D_2O})_0$=0.0057–0.0383 mol/mol at p_0=59.7 kPa.[59] This fact can be explained qualitatively by the nature of the nucleation in the nozzle flow as follows. The nucleation rate first increases as the temperature decreases, and after the onset of condensation, nucleation is quenched due to the monomer depletion and the increase in temperature resulting from latent heat release into the gas. The number density of the nucleus is kept at almost constant by this self-control mechanism.

In Refs. 6, 59, and 60, the results of the number density of the droplet at the measuring point are described in the unit of cm^{-3}. However, this value changes along the flow even after the end of the nucleation because the gas density changes. Hence, in this appendix, the mole fraction of the droplets, $y_{drop} \equiv N/N_A/(p/RT)$, will be used, where N_A is Avogadro's number.

The reported value[59] of y_{drop} of D_2O in the nozzle A($d(A/A^*)/dz$=0.049 cm^{-1}) measured by small angle newtron scattering (SANS) measurement at T_0=298.2, 308.2, and 318.2 K, and that value[60] of nonane in nozzle C($d(A/A^*)/dz$=0.079 cm^{-1}) measured by SAXS at T_0 =298.2 and 308.2 K, help us estimate the T_0 dependence of the y_{drop} of EtOD/D_2O in nozzle H($d(A/A^*)/dz$ =0.054 cm^{-1}) in the present study. We compare the T_0 dependencies of y_{drop} in the three different nozzles under the condition that the isentropic cooling rates (dT_{is}/dt) at the onset points are the same. This criterion does not necessarily cancel out the difference of the expansion rate of the nozzle. However, we can expect that the T_0 dependence of y_{drop} of EtOD/D_2O in nozzle H is intermediate between those of D_2O (polar molecule) in nozzle A and nonane (nonpolar molecule) in nozzle C, because ethanol is an amphiphilic molecule and nozzle H has a middle expansion rate between nozzle A and nozzle C.

At the onset point of EtOD/D_2O condensation in nozzle H, z=1.36 cm (see Appendix D 1), dT_{is}/dt is −4.5 ×10^5 K/s. In nozzle A, the cooling rate takes the same value at z=1.2 cm, and when onset occur at this position, it was estimated from the data in Ref. 59 that y_{drop} increases by 19% with the increase in T_0 from 298.2 to 308.2 K. A similar estimation was done for nonane nucleation in nozzle C, and y_{drop} is expected to increase by 20% when T_0 is increased from 298.2 to 308.2 K. Therefore, y_{drop} of EtOD/D_2O in Nozzle H in LAM (T_0=303.7 K) is expected to be lower than that in XSM (T_0=308.2 K) by 9% (≈19.5% ×4.5 K/10 K).

3. Droplet growth rates

As expected in Appendix D 1, the onset position in XSM (T_0=308.2 K) is 0.34 cm downstream of that in LAM (T_0 =303.7 K). In order to estimate the difference in the growth rates of the droplets in the LAM at $z \geq 1.36$ cm and in the XSM at $z \geq 1.70$ cm, $T_{is}(z)$ and $p_{vis}(z)$ in LAM are compared with $T_{is}(z+0.34)$ and $p_{vis}(z+0.34)$ in XSM, respectively, in Fig. 12. The difference of T_{is} is less than 1 K downstream of the onset point (z=1.36 cm). $p_{vis}(z)$ in LAM is higher than

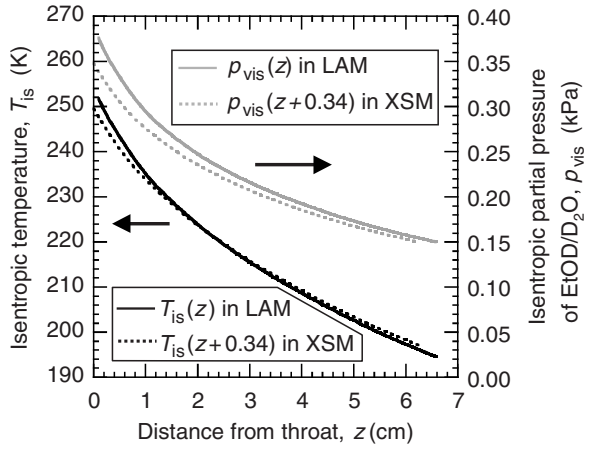

FIG. 12. Comparison of the isentropic temperatures, T_{is}, or the partial pressures of the condensable species, p_{vis}, between the LAM and XSM.

$p_{vis}(z+0.34)$ in XSM by 6% at $z=1.36$ cm, and by 3% at $z=6.00$ cm. These results are listed in Table II with the results of other variables.

The difference of the growth rate, $\Delta(dn/dz)$, where n is the number of molecules in a droplet and the operator Δ is defined in the caption of Table II, is approximated assuming $\Delta T=0$ as

$$\begin{aligned}\Delta(dn/dz) &\approx \Delta(dn/dt) - \Delta(dz/dt)\\ &\approx \Delta p_{vis} - \Delta u_{is}\\ &\approx (0.06+0.03)/2 + (0.03+0.01)/2\\ &\approx 0.07. \end{aligned} \quad \text{(D1)}$$

The difference of the temperature increase by condensation is estimated as

$$\begin{aligned}\Delta\{d(T-T_{is})/dz\} &\approx \Delta\{y_{drop}(dn/dz)\}\\ &\approx \Delta y_{drop} + \Delta(dn/dz)\\ &\approx -0.09 + 0.07\\ &= -0.02. \end{aligned} \quad \text{(D2)}$$

Hence, the temperature in LAM is expected to be slightly lower than that in XSM considering $\Delta T_{is}\approx 0$, and therefore $\Delta(dn/dz)$ should be slightly larger than Eq. (D1) because the evaporation rate of monomers from the droplets decreases with a decrease in T. However, the true value of $\Delta(dn/dz)$ should not exceed 0.09 because the value of Eq. (D2) becomes zero when $\Delta(dn/dz)=0.09$. Therefore, the difference of the radius of the droplet between LAM and XSM, $\Delta r(\approx \Delta n/3)$ is expected to be less than $0.09/3=0.03$. When the same method was applied to the values at each position, $z=1.36$ or 6.00 cm, without averaging, the same result was obtained both at $z=1.36$ and 6.00 cm.

As discussed in this appendix, the radius of the droplet, $r(z)$, in LAM is expected to be larger than $r(z+0.34$ cm) measured in XSM only by less than 3%. We found the increase in r by 3% causes the increase in Δh_{theor} in Fig. 6(c) by up to 0.3% and by 0.06% on average, and these changes are negligibly small. Therefore, we can use the radius of the droplet measured by XSM for analysis in this study only by shifting the position 0.34 cm upstream.

APPENDIX E: CORRECTION FOR TEMPERATURE DIFFERENCE BETWEEN THE TWO PTM

As discussed in the previous paper[4] and in Appendix D, T_0 in the PTM is expected to range from 303.2 to 306.2 K even though the temperature measured by RTD in plenum, $(T_0)_{RTD}$, was kept at 308.2 K because of a bypass flow problem in the plenum. In the case of PTM of the EtOD/D_2O flow, T_0 is expected to be 303.7 K because T_0 in the flow of the same composition was spectroscopically measured to be 303.7 K in the LAM. Therefore, onset position in the pure EtOD flow at $T_0=303.7$ K should be compared with that in the EtOD/D_2O flow to investigate the effect of D_2O on the phase change of EtOD. However, in the case of the pure EtOD flow at $(y_{EtOD})_0=0.0097$, spectroscopic temperature was not measured, and, therefore, we should consider the uncertainty of T_0, which is expected to range from 303.2 to 306.2 K. The onset position of the deviation of p from p_{is}, z_{on_p}, in the pure EtOD flow at $T_0=303.7$ K was estimated as follows. In the previous study,[4] PTM and LAM of a pure EtOD flow with $(y_{EtOD})_0=0.0080$ were performed and T_0 was determined to be 303.2 K by LAM. From these results, the onset condition (temperature and partial pressure of EtOD) for the deviation of p from p_{is} was determined as $T_{on\_p}=218.8$ K and $p_{EtOD\_on\_p}=0.075$ kPa. Furthermore, from the result of PTM of pure EtOD flow in Fig. 4, the onset condition was determined as $T_{on\_p}=223.2\sim225.4$ K and $p_{EtOD\_on\_p}=0.099$ kPa, considering that $T_0=303.2\sim306.2$ K. On the assumption that there is a linear relation between $\ln(p_{EtOD\_on\_p})$ and T_{on_p}, two straight lines were drawn, which connect $\{T_{on\_p},\ln(p_{EtOD\_on\_p})\}$ at $(y_{EtOD})_0=0.0080$ and [maximum or minimum of T_{on_p}, $\ln(p_{EtOD\_on\_p})$] at $(y_{EtOD})_0=0.0097$. The wet isentropic curve for the EtOD/D_2O flow, $\ln(p_{EtOD\_is})$ versus T_{is}, was drawn and the two intersections of this curve and the two straight lines, $\ln(p_{EtOD\_on\_p})$ versus T_{on_p}, were determined. These two intersections let us bind the region where onset is expected to occur in the EtOD/D_2O flow at $T_0=303.7$ K if the phase change of EtOD is not affected by D_2O. The predicted

TABLE II. Differences of the conditions between LAM and XSM. Here, Δy_{drop} is defined by $\Delta y_{drop} \equiv [\{y_{drop}(z) \text{ in LAM}\}-\{y_{drop}(z+0.34 \text{ cm}) \text{ in XSM}\}]/\{y_{drop}(z+0.34 \text{ cm}) \text{ in XSM}\}$, and other values, Δp_{is}, Δp_{vis}, Δu_{is}, ΔT_{is}, are defined similarly. u_{is} is the velocity of the gas in the isentropic flow.

Δy_{drop} [a]	$\Delta p_{is}=\Delta p_{vis}$		Δu_{is}		ΔT_{is}	
$z\geq 1.36$ cm	$z=1.36$	$z=6.00$	$z=1.36$	$z=6.00$	$z=1.36$	$z=6.00$
−0.09	0.06	0.03	−0.03	−0.01	0.003	−0.005

[a]This value was estimated in Appendix D 2.

region was $z_{on\_p}=1.7\sim2.1$ cm, which is 0.6–1.0 cm downstream from the onset position ($z_{on\_p}=1.1$ cm) measured in the actual EtOD/D_2O flow. Furthermore, we found that the line for the EtOD/D_2O flow, $\ln(p_{\nu\text{-EtOD}})$ versus T intersects with neither of the two lines, $\ln(p_{\text{EtOD\_on\_}p})$ versus T_{on_p}, where $p_{\nu\text{-EtOD}}$ denotes the partial pressure of EtOD. That is, the phase change (condensation and/or clustering) of pure EtOD cannot occur in the EtOD/D_2O flow under the conditions of this study without the contribution of D_2O.

APPENDIX F: ESTIMATING THE RADIUS OF THE DROPLET IN THE D_2O CONDENSING FLOW

To estimate Δh_{theor} in Fig. 7(b), we used the mean radius of the H_2O droplets measured by SAXS (Ref. 5) in the nozzle H2, which has the same A/A^* profile as the nozzle H used in the present study. This approximation is not expected to affect the comparison between the Δh_{exp} and Δh_{theor} in Fig. 7(b) as explained below.

The mean radius of the H_2O droplets was measured in the condensation flow with $T_0=298$ K, $p_0=30$ kPa, and $(y_{H_2O})_0=0.033$, where, according to the PTM, the onset position of condensation is the same as that in the D_2O condensing flow [$T_0=298.2$ K, $p_0=30.1$ kPa, and $(y_{D_2O})_0=0.025$], and the profile of the mass fraction of condensate of H_2O, g_{H_2O}, agrees with that of D_2O within the error range 0 to +5%. Because the density of H_2O liquid is lower than that of D_2O liquid by about 10%, the volume of the condensed H_2O in nozzle H2 is expected to be higher than that of the D_2O condensed in nozzle H by about 15% (=10%+5%). It was found by SANS (Ref. 61) that the nucleation rates are the same in the supersonic nozzle flows of H_2O and D_2O, which give the same onset position at the same T_0, same p_0, and different $(y_v)_0$. Therefore, the number of nuclei in the two condensing flows is expected to be the same. The volume of a H_2O droplet is expected to be larger than that of a D_2O droplet by about 15%, and, hence, the radius of H_2O droplet is expected to be larger than that of D_2O droplet by about 5%, which causes the increase in Δh_{theor} in Fig. 7(b) only by up to 0.5% and by 0.1% in average, and these changes are negligibly small. The H_2O droplet radius data measured by SAXS were fitted by $r=a_0+a_1(1/z)+a_2(1/z)^2+a_3(1/z)^3$ and extrapolated as shown in Fig. 7(a).

APPENDIX G: EQUILIBRIUM CONSTANTS AND HEAT OF DISSOCIATION OF THE DIMERS, $(EtOH)_2$, $(EtOH)(H_2O)$, AND $(H_2O)_2$, DERIVED FROM THE SECOND VIRIAL COEFFICIENTS

The second virial coefficient of a binary mixture, B_M, is expressed by[18,62]

$$B_M=(y_1)^2B_{11}+2y_1(1-y_1)B_{12}+(1-y_1)^2B_{22}, \quad \text{(G1)}$$

where y_1 is the mole fraction of the species 1, B_{12} denotes the second cross virial coefficient between species 1 and 2, and B_{11} and B_{22} are the second virial coefficients of species 1 and 2, respectively. The second virial coefficients are related to the equilibrium constants for the formations of the dimers as[13,62]

$$B_{ii}=b_i-RTK_{2(ii)}, \quad i=1,2, \quad \text{(G2)}$$

$$B_{12}=b_{12}-RTK_{2(12)}/2, \quad \text{(G3)}$$

where b_i is the excluded volume (covolume) of the monomer of species i. $K_{2(ii)}$ and $K_{2(12)}$ are the equilibrium constants for the formation of the pure dimer and the hetero dimer, respectively. The covolume for B_{12}, $b_{12}=(b_1+b_2)/2$ was obtained by applying the arithmetic-mean rule. The temperature dependence of the equilibrium constant is expressed by the enthalpy of dissociation of the dimer as

$$K_{2(ij)}(T)=K_{2(ij)}(T_0)\exp[(1/T-1/T_0)\Delta H_{2(ij)}/R], \quad \text{(G4)}$$

where $\Delta H_{2(ij)}$ is the enthalpy of dissociation of the dimer of species i and j. Therefore, $\Delta H_{2(ij)}$ can be determined from the slope of the line, $R\ln\{-(B_{ii}-b_i)/RT\}$ versus $1/T$, for pure dimer, and, for heterodimer, from the slope of the line, $R\ln\{-(2B_{12}-b_1-b_2)/RT\}$ versus $1/T$. $K_{2(ij)}(T_0)$ is also determined from the fitting.

Noppe *et al.*[18] measured B_M of EtOH/H_2O vapor mixtures in the temperature range from 400 to 525 K, and determined B_{12} using the literature values of B_{11} and B_{22}, which are also shown in their paper. For the excluded volume of EtOH and H_2O, we used the literature values of the Van der Waals covolume,[48] $b_{EtOH}=87.1$ cm^3 mol^{-1} and $b_{H2O}=30.5$ cm^3 mol^{-1}, and $\{K_{2(ij)}(298.2\text{ K})/\text{MPa}^{-1}, \Delta H_{2(ij)}/\text{kJ mol}^{-1}\}$ were determined as follows: {0.86, 15.0} for $(EtOH)_2$, {0.50, 14.4} for $(H_2O)_2$, and {1.19, 14.1} for $(EtOH)(H_2O)$.

[1] B. E. Wyslouzil, C. H. Heath, J. L. Cheung, and G. Wilemski, J. Chem. Phys. **113**, 7317 (2000).
[2] P. Paci, Y. Zvinevich, S. Tanimura, B. E. Wyslouzil, M. Zahniser, J. Shorter, D. Nelson, and B. McManus, J. Chem. Phys. **121**, 9964 (2004).
[3] S. Tanimura, Y. Zvinevich, B. E. Wyslouzil, M. Zahniser, J. Shorter, D. Nelson, and B. McManus, J. Chem. Phys. **122**, 194304 (2005).
[4] S. Tanimura, B. E. Wyslouzil, M. Zahniser, J. Shorter, D. Nelson, and J. B. McManus, J. Chem. Phys. **127**, 034305 (2007).
[5] B. E. Wyslouzil, G. Wilemski, R. Strey, S. Seifert, and R. E. Winans, Phys. Chem. Chem. Phys. **9**, 5353 (2007).
[6] Y. J. Kim, B. E. Wyslouzil, G. Wilemski, J. Wölk, and R. Strey, J. Phys. Chem. A **108**, 4365 (2004).
[7] B. E. Wyslouzil, G. Wilemski, R. Strey, C. H. Heath, and U. Diregsweiler, Phys. Chem. Chem. Phys. **8**, 54 (2006).
[8] N. Nishi, K. Koga, C. Ohshima, K. Yamamoto, U. Nagashima, and K. Nagami, J. Am. Chem. Soc. **110**, 5246 (1988).
[9] A. Wakisaka and T. Ohki, Faraday Discuss. **129**, 231 (2005).
[10] M. Kotlarchyk and S. H. Chen, J. Chem. Phys. **79**, 2461 (1983).
[11] (a) H. W. Liepmann and A. Roshko, *Elements of Gasdynamics* (Dover, New York, 2002), Chap. 2; (b) H. W. Liepmann and A. Roshko, *Elements of Gasdynamics* (Dover, New York, 2002), Chap. 13, Sec. 13.11.
[12] Kirchhoff's equation is an approximate form of Planck's equation, that is, the pressure dependence of the heat of vaporization is neglected in the Kirchhoff's equation. See K. Denbigh, *The Principles of Chemical Equilibrium*, 3rd ed. (Cambridge University Press, London, 1971), pp. 145 and 201.
[13] M. Massucci, M. M. von Kralik, and C. J. Wormald, J. Chem. Soc., Faraday Trans. **88**, 985 (1992).
[14] A. Laaksonen and M. Kulmala, J. Chem. Phys. **95**, 6745 (1991).
[15] S. Matsuo, T. Setoguchi, S. Yu, and K. Matsuo, J. Therm. Sci. **6**, 260 (1997).
[16] G. M. Barrow, J. Chem. Phys. **20**, 1739 (1952).
[17] J. F. Counsell, J. O. Fenwick, and E. B. Lees, J. Chem. Thermodyn. **2**, 367 (1970).
[18] R. Noppe, M. Ramsdorf, W. Lichtenstein, and G. Opel, Z. Phys. Chem. (Leipzig) **262**, 1157 (1981).
[19] S. M. Mejía, J. F. Espinal, A. Restrepo, and F. Mondragón, J. Phys. Chem. A **111**, 8250 (2007).
[20] M. Sato, K. Matsuura, and T. Fujii, J. Chem. Phys. **114**, 2382 (2001).

[21] Y. F. Yano, K. Matsuura, T. Fukazu, F. Abe, A. Wakisaka, H. Kobara, K. Kaneko, A. Kumagai, Y. Katsuya, and M. Tanaka, J. Chem. Phys. **127**, 031101 (2007).
[22] S. H. Bauer and C. F. Wilcox, Jr., J. Phys. Chem. **98**, 8721 (1994).
[23] W. J. Moore, *Physical Chemistry*, 5th ed. (Longman, Singapore, 1972), Sec. 22.
[24] D. Ben-Amotz and D. R. Herschbach, J. Phys. Chem. **94**, 1038 (1990).
[25] M. L. Senent, Y. G. Smeyers, and R. Domínguez-Gómez, in *Progress in Theoretical Chemistry and Physics*, edited by J. Maruani and S. Wilson (Kluwer, Boston, 1999), Vol. 6, pp. 359–374.
[26] M. Ehbrecht and F. Huisken, J. Phys. Chem. A **101**, 7768 (1997).
[27] S. Coussan, M. E. Alikhani, J. P. Perchard, and W. Q. Zheng, J. Phys. Chem. A **104**, 5475 (2000).
[28] NIST Chemistry WebBook, http://webbook.nist.gov/chemistry/.
[29] H. Schlichting and K. Gersten, *Boundary Layer Theory*, 8th ed. (Springer, Berlin, 2000), Chaps. 2.6, 6.2, and 15.2.4b.
[30] B. S. Stratford, J. Fluid Mech. **5**, 1 (1959).
[31] S. Ono and S. Kondo, in *Encyclopedia of Physics*, edited by S. Flügge (Springer, Berlin, 1960), Vol. 10, p. 134.
[32] F. P. Buff, Z. Elektrochem. **56**, 311 (1952); F. O. Koenig, J. Chem. Phys. **18**, 449 (1950).
[33] J. H. Seinfeld and S. N. Pandis, *Atmospheric Chemistry and Physics: From Air Pollution to Climate Change* (Wiley, New York, 1997), Chap. 8.
[34] E. H. Kennard, *Kinetic Theory of Gases* (McGraw-Hill, New York, 1938), pp. 312–315.
[35] *Enthalpies of Vaporization of Organic Compounds: A Critical Review and Data Compilation*, edited by V. Majer and V. Svoboda (Blackwell Scientific, Oxford, 1985), Sec. 5.2.1.
[36] T. Schmeling and R. Strey, Ber. Bunsenges. Phys. Chem. **87**, 871 (1983).
[37] I. Kiss, Gy. Jákli, G. Jancsó, and H. Illy, J. Chem. Phys. **47**, 4851 (1967).
[38] E. Z. Zhuravlev and I. B. Rabinovich, Trudy po Khimii i Khimicheskoi Tekhnologii **2**, 475 (1959).
[39] P. N. Nikolaev, I. B. Rabinovich, and B. V. Lebedev, Russ. J. Phys. Chem. **41**, 688 (1967).
[40] P. G. Hill, R. D. C. MacMillan, and V. Lee, J. Phys. Chem. Ref. Data **11**, 1 (1982).
[41] G. F. Kraus and S. C. Greer, J. Phys. Chem. **88**, 4781 (1984).
[42] A. S. Friedman and L. Haar, J. Chem. Phys. **22**, 2051 (1954).
[43] S. B. Kiselev and J. F. Ely, J. Chem. Phys. **118**, 680 (2003).
[44] J. H. S. Green, Trans. Faraday Soc. **57**, 2132 (1961).
[45] D. M. Murphy and T. Koop, Q. J. R. Meteorol. Soc. **131**, 1539 (2005).
[46] G. Archer and R. W. Carter, J. Phys. Chem. B **104**, 8563 (2000).
[47] *Lange's Handbook of Chemistry*, 14th ed., edited by J. A. Dean (McGraw-Hill, New York, 1992).
[48] *Handbook of Chemistry and Physics*, 84th ed., edited by D. R. Lide (CRC, Boston, 2003).
[49] U. Dieregsweiler, Thesis, Worcester Polytechnic Institute, Worcester, 2001.
[50] C. M. Sorensen, J. Chem. Phys. **79**, 1455 (1983).
[51] T. S. Khasanshin and A. A. Aleksandrov, Inzh.-Fiz. Zh. **47**, 411 (1984).
[52] J. J. Jasper, J. Phys. Chem. Ref. Data **1**, 841 (1972).
[53] J. Timmermans, *The Physico-Chemical Constants of Binary Systems in Concentrated Solutions* (Interscience, New York, 1960), Vol. 4, p. 197.
[54] A. W. Adamson, *Physical Chemistry of Surfaces*, 2nd ed. (Interscience, New York, 1967).
[55] A. Chand and D. V. Fenby, J. Chem. Thermodyn. **10**, 997 (1978).
[56] J. J. Christensen, R. W. Hanks, and R. M. Izatt, *Handbook of Heats of Mixing* (Wiley, New York, 1982), Table W78.
[57] P. Westh and A. Hvidt, Biophys. Chem. **46**, 27 (1993).
[58] S. Westmeier, Chem. Tech. (Leipzig) **28**, 350 (1976).
[59] A. Khan, C. H. Heath, U. M. Dieregsweiler, and B. Wyslouzil, J. Chem. Phys. **119**, 3138 (2003).
[60] D. Ghosh, D. Bergmann, R. Schwering, J. Wölk, R. Strey, S. Tanimura, and B. E. Wyslouzil, J. Chem. Phys. **132**, 024307 (2010).
[61] C. H. Heath, K. A. Streletzky, B. E. Wyslouzil, J. Wölk, and R. Strey, J. Chem. Phys. **118**, 5465 (2003).
[62] C. J. Wormald, N. M. Lancaster, and C. J. Sowden, J. Chem. Soc., Faraday Trans. **93**, 1921 (1997).